Master's Thesis

Optical discrimination among dinoflagellate species causing Harmful Algal Blooms (HABs) in Korean coastal waters

한국 연안에서 발생하는 와편모조류 유해 적조의 광학적 구별

Advisor : Professor Sinjae Yoo

Co-advisor: Professor Dongseon Kim

Yeseul Kim

Department of Convergence Study on the Ocean Science and Technology

Ocean Science and Technology School

February 2017

본 논문을 김예슬의 이학석사 학위논문으로 인준함.

위원장	손 영 백	(인)
위 원	유 신 재	(인)
위 원	김 동 선	(인)

2016년 11월 30일

한국해양대학교 해양과학기술전문대학원

Contents

List of Tables

List of Figures

List of Abbreviations

AOPs	Apparent Optical Properties
a	Absorption coefficient
a_{dm}	Detritus/mineral absorption coefficient
a_g	Colored Dissolved Organic Matter absorption coefficient
a_p	Particulate absorption coefficient
a_{ph}	Phytoplankton absorption coefficient
a_w	Seawater absorption coefficient
a^*_{ph}	Chlorophyll a specific absorption coefficient
$a^*_{ph}/a^*_{ph}(440)$	a^*_{ph} normalized to 440 nm
$\hat{a}_{ph}$	Mean absorption coefficient
$\hat{a}_{nph}$	Mean normalized absorption coefficient
b	Scattering coefficient
b_b	Backscattering coefficient
b_{bdm}	Detritus/mineral backscattering coefficient
b_{bdm}/b_{dm}	Detritus/mineral backscattering ratio
b_{bph}	Phytoplankton backscattering coefficient
b_{bph}/b_{ph}	Phytoplankton backscattering ratio
b_{bw}	Seawater backscattering coefficient
CDOM	Colored Dissolved Organic Matter
Chl *a*	Chlorophyll a concentration
E_d	Downwelling irradiance
HABs	Harmful Algal Blooms
IOCCG	International Ocean-Color Coordinating Group
IOPs	Inherent Optical Properties
KIOST	Korea Institute Ocean Science and Technology
L_u	Upwelling radiance
L_w	Water-leaving radiance
MODIS	Moderate Resolution Imaging Spectroradiometer
NIR	Near-infrared region
NFRDI	National Fisheries Research and Development Institute

O.D	Optical density
R_{rs}	Remote sensing reflectance
R_{rs} ratios	$R_{rs}(\lambda_2)/R_{rs}(\lambda_1)$ ($\lambda_2 > \lambda_1$)
R_1	$R_{rs}(555)/R_{rs}(531)$
R_2	$R_{rs}(488)/R_{rs}(443)$
SI	Similarity Index
S_{dm}	Spectral slope of $a_{dm}(\lambda)$
S_g	Spectral slope of $a_g(\lambda)$
UPA	Unspecified Phytoplankton Assemblages

한국 연안에서 발생하는 와편모조류 유해 적조의 광학적 구별

김 예 슬

한국해양대학교 해양과학기술전문대학원
해양과학기술융합학과

요 약

이 연구는 한국 연안에서 발생하는 유해 적조(Harmful Algal blooms)를 광학적으로 구별하는 방법을 개발하기 위해 진행되었으며, 특히 주요 유해 적조 원인 종으로 알려진 와편모조류 *Cochlodinium polykrikoides*에 초점을 맞추어 생물 광학적 특성을 활용한 적조 탐지 가능성에 대한 연구를 하였다. 이 연구에서는 실험실에서 배양 중인 *C. polykrikoides*를 비롯한 다른 와편모조류 유해 적조 종들의 흡광 스펙트럼을 측정하여 적조 종이 가지는 고유한 흡광 특성을 파악하였다. 또한 유해 적조 종의 고유 광 특성 의한 반사도 스펙트럼의 분광 반응을 바탕으로 광학적 구별 방법을 제시하였다. 연구에 활용된 반사도 스펙트럼(N = 2,275)은 실험으로 측정한 적조 종 흡광 자료와 International Ocean-Color Coordinating Group에서 제공하는 자료를 사용하여 광학 모델인 Hydrolight를 통해 모의되었다. 해수의 반사도에 영향을 미치는 해수 구성요소의 농도를 다양하게 설정하여 폭넓은 광학적 조건

을 포괄하는 2,275개의 반사도 스펙트럼을 생성하였다.

모의 된 반사도 스펙트럼 자료를 분석한 결과, *C. polykrikoides*를 포함한 4 종의 유해 적조 종의 반사도 스펙트럼 간에는 높은 유사도를 보인 반면, 적조가 아닌 경우의 반사도와 적조인 경우의 반사도는 뚜렷한 차이를 보였다. 특히, *C. polykrikoides* 적조인 경우에 청-녹 파장에서 보이는 고유한 흡광 특성이 반사도에 영향을 줌으로써 적조가 아닌 경우의 반사도와 구별되는 특징을 보였고 이 차이를 바탕으로 *C. polykrikoides* 구별 방법을 제시하였다. R_1: $R_{rs}(555)/R_{rs}(531)$와 R_2: $R_{rs}(488)/R_{rs}(443)$, 두 반사도 밴드 비를 사용하여 적조가 아닌 경우로부터 효과적으로 *C. polykrikoides* blooms를 구별할 수 있었다. 모의 된 반사도 자료를 바탕으로 제안 된 두 반사도 밴드 비를 실제 한국 연안에서 측정한 반사도에 적용한 결과, *C. polykrikoides* 적조와 적조가 아닌 해역이 명확히 구별되었다.

한국 연안에서 발생하는 유해 적조 종의 광 특성 및 이를 바탕으로 제안 된 반사도 밴드 비 구별 방법 등의 분석 결과들은 추후 in-water 적조 탐지 알고리듬 및 위성 적조 탐지 알고리듬 개발을 위한 이론적, 정량적 기준을 제공할 수 있을 것으로 기대된다.

KEY WORDS: 유해 적조; 적조 탐지; *Cochlodinium polykrikoides*, 흡광계수; 위성 반사도; 한국 연안

Optical discrimination among dinoflagellate species causing Harmful Algal Blooms (HABs) in Korean coastal waters

Yeseul Kim

Department of Convergence Study on the Ocean Science and Technology
Ocean Science and Technology School

Abstract

We investigated the possibility of optically discriminating harmful algal blooms (HABs) focusing on *Cochlodinium polykrikoides*, the major HAB causative dinoflagellate species in Korean waters. Our aim is to define the bio-optical characteristics of *C. polykrikoides* and other dinoflagellate species blooms in order to develop the optical discrimination method based on the spectral response of remote sensing reflectance (R_{rs}). We produced a large dataset (N = 2,275) of simulated R_{rs} spectra in a wide range of bio-optical conditions using Hydrolight software and bio-optical data provided by the International Ocean-Color Coordinating Group. We identified the spectral differences of R_{rs} associated with the distinct absorption characteristics for *C. polykrikoides* in the blue-green wavelength. The two R_{rs} band ratios (R_1: $R_{rs}(555)/R_{rs}(531)$ and R_2:

$R_{rs}(488)/R_{rs}(443)$) were determined to be effective in discriminating *C. polykrikoides* blooms. *C. polykrikoides* clearly occupy separated subspace in the 2-D space of R_1 and R_2. The results were consistent with *in situ* observations and seem applicable to diverse coastal environments. Our findings provide theoretical and quantitative criteria upon which in-water HAB detecting algorithms can be developed. Such algorithms can be extended to satellite remote sensing providing synoptic monitoring tools for detecting HABs in a large expanse of water.

KEY WORDS: Harmful Algal Blooms (HABs); red tide detection; *Cochlodinium polykrikoides*; absorption coefficient; remote sensing reflectance; Korean coastal waters

Chapter 1 Introduction

1.1 Background

Over the past decades, harmful algal blooms (HABs) have been a significant threat to fishery industries, humans, and economies worldwide (Gobler *et al*., 2012). HABs are a national concern because they affect not only the health of people but also the health of marine ecosystems. While we know of many factors that may contribute to HABs, how these factors come together to create a HABs is not well understood. So, it is important to determine the outbreak mechanism of HABs and to develop the early HABs warning and forecasting system for controlling HABs and preventing huge damages.

Many researchers have continued to monitor and study HABs for a number of years to determine how to forecast the location of the blooms. To detect and monitor the spatio-temporal distributions, and propagation of HABs, field observations, oceanographic monitoring platforms such as buoys, glider data, and satellite remote sensing have been employed (Son *et al*., 2011; Ahn & Shanmugam, 2006). Currently, *in situ* observations (e.g., examination of discrete water samples) are considered as the principal detection method in limited areas, but are labor intensive, slow, and intermittent (Roelke *et al*., 1999; Kirkpatrick *et al*., 2000). Developing feasible approaches for the synoptic monitoring and early detection of widespread HABs is highly desirable to mitigate the losses of the fishing industry, assist in fishery management, and enhance the tourism industry (Shang *et al*., 2014; Craig *et al*., 2006). Most of all, satellite remote sensing of the ocean color has become an increasingly important and powerful tool for detecting the distribution of HABs and phytoplankton groups based on optical signatures because of its extensive spatial and temporal coverage (Shang *et al.*, 2014; Choi *et al.*, 2014; Cannizzaro *et al.*, 2008; Kurekin *et al.*, 2014; Alvain *et al.*, 2008). For the effective application of ocean color remote sensing, several remote sensing techniques were developed (Stumpf, 2003; Ahn & Shanmugam, 2006; Lubac *et al.*, 2008; Shang *et al.*, 2014; Wynne *et al.*, 2008; Sasaki *et al.*, 2008; Xi *et al.*, 2015).

Satellite-derived chlorophyll a (Chl *a*) concentrations have been used to detect HABs as a proxy for phytoplankton biomass (Tomlinson *et al.*, 2004; Ishizaka *et al.*, 2006). However, the accurate discrimination between HABs and non-HABs is not feasible based only on high Chl *a* concentrations because all phytoplankton contains this photosynthetic pigment (Roelke *et al.*, 1999; Siswanto *et al.*, 2013). The standard satellite Chl *a* algorithm (O'Reilly *et al.*, 2000), the blue-to-green band ratio, provides reasonable estimates for Case 1 water, but not for Case 2 water. The presence of suspended sediment and colored dissolved organic matter (CDOM) causes an increase in absorption and/or scattering, which over-estimates Chl *a* as red tide water (Ahn and Shanmugam, 2006; Hu *et al.*, 2005).

In an attempt to develop HABs detection methods based on bio-optical approaches, a red tide index associated with the band ratio method was proposed in Ahn and Shanmugam (2006). However, the empirical nature of this index requires the determination of an arbitrary coefficient that strongly affects the outcome. Other attempts have utilized the spectral signatures of the bio-optical properties of HAB species to identify blooms (Cannizzaro *et al.*, 2008; Xi *et al.*, 2015; Lubac *et al.*, 2008). The usefulness of these approaches depends on the comprehensive understanding of unusual spectral signatures of inherent optical properties (IOPs) exhibited by algal groups (Kirkpatrick *et al.*, 2000; Millie *et al.*, 1997). Some of these methods use the spectral characteristics of phytoplankton absorption ($a_{ph}(\lambda)$). In general, HABs in optically complex waters are characterized by increased absorption and have lower blue reflectance than the non-bloom waters. The distinctive reflectance patterns of HABs also reflect their bio-optical properties (Shang *et al.*, 2014), which can be used to distinguish them from blooms formed by other organisms based on the spectral response method (Lubac *et al.*, 2008; Guzmán *et al.*, 2016). In Lubac *et al.* (2008), both the hyperspectral and multispectral analysis methods were used to explore the applicability of $a_{ph}(\lambda)$ and remote sensing reflectance ($R_{rs}(\lambda)$) for the discrimination of *Phaeocystis globosa* blooms from diatom blooms. These approaches based on bio-optical closure relationships might be useful to accurately discriminate HABs. Furthermore, a species identification is expected to be possible based on distinct optical properties.

1.2 Problem statement

In Korean coastal waters, dinoflagellates are known as the major causative species that forms HABs since the 1990s (Lee *et al.*, 2013). Specifically, blooms of the dinoflagellate *Cochlodinium polykrikoides* have been frequently observed in the southern coast of Korea during the summer and autumn seasons since 1985 and have caused significant damages to the aquaculture industry (Lee *et al.*, 2013) (Fig. 3). *C. polykrikoides* blooms caused fish kills of 746 hundred million KRW in 1995 (the largest fish kill) as resulting in suffocation associated with structural and functional changes at the gill filament. Through the 2000s, *C. polykrikoides* was the single most important species causing fish kills in Korea (Lee *et al.*, 2014). These blooms are geographically unconstrained and extend into turbid water in the west coast and/or into clear water in the east coast of Korea (Suh *et al.*, 2004) (Fig. 2).

Case 1 waters (clear waters) are those waters in which phytoplankton are the principal agents responsible for variations in optical properties of the water. On the other hand, Case 2 waters such as turbid waters are influenced not just by phytoplankton and related detritus/mineral, but also by CDOM (IOCCG, 2000). The southern coast of Korea that belong to Case 2 waters is the main place of origin of *C. polykrikoides* blooms. *C. polykrikoides* bloomsexpand into west and/or east coast because these blooms flourish when wind and ocean currents are favorable. In order to develop the detection method of HABs in Korean coastal waters, we need to understand the optical conditions of waters around the Korean Peninsula.

In Son *et al.* (2011), a systematic classification method considering optical conditions of waters was suggested for distinguishing waters with *C. polykrikoides* blooms from non-bloom waters based on four different criteria using Moderate Resolution Imaging Spectroradiometer (MODIS) satellite data. Because this is an empirical algorithm its applicability is rather limited and it has not been applied in real-world situation.

Although recent researches have obtained the optical properties of bloom waters using satellite and *in situ* data, few studies have been performed on the detection of *C. polykrikoides* blooms using the satellite remote sensing technique based on the bio-optical properties of *C. polykrikoides* blooms in Korean coastal waters. Besides, little study on comprehensive understanding of optical properties by *C. polykrikoides* under various optical conditions has been conducted.

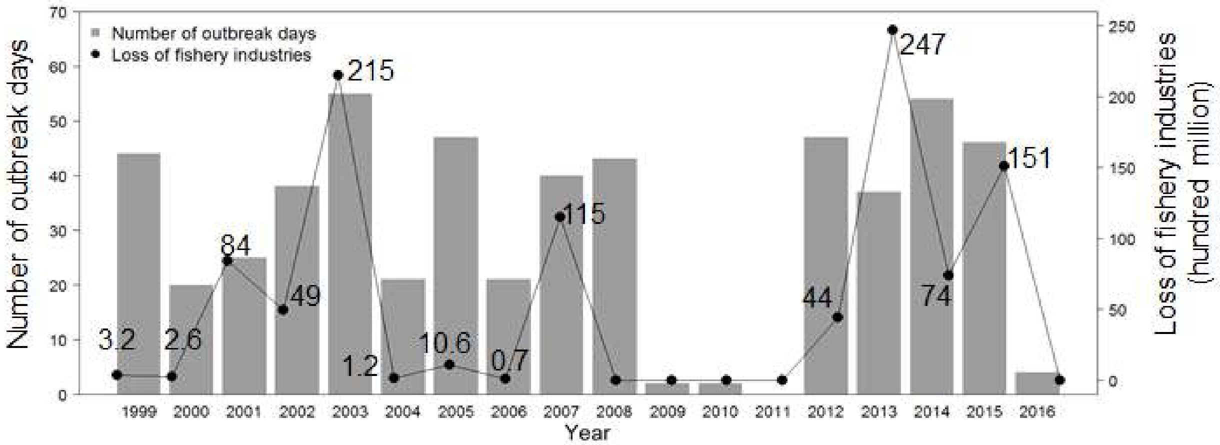

Fig. 2 Historical records of *C. polykrikoides* blooms in Korea. The number of outbreak days (grey bars) and loss of fishery industries (black circles) in Korea from 1999 to 2016 were reported by NFRDI of Korea. The number of outbreak days is estimated by the total days for which the red tide alert (higher than 1,000 cells/ml) has been issued.

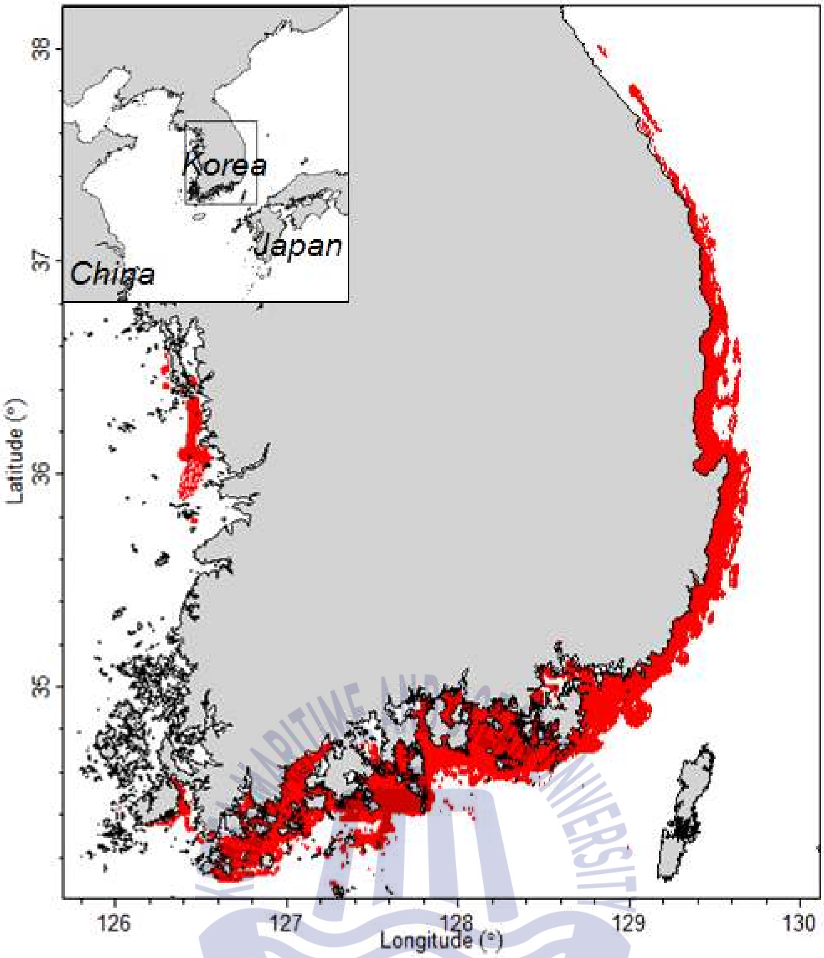

Fig. 3 The spatial distribution of *C. polykrikoides* blooms (red points) in the seas around the Korean Peninsula during 1998~2016. Spatial information of blooms was extracted from HAB outbreak reports by NFRDI.

1.3 Research aim and approach

The goal of our study is to explore the possibility of optically discriminating harmful *C. polykrikoides* blooms from non-HABs and/or other dinoflagellate HABs species including *Akashiwo sanguinea, Alexandrium tamarense, and Scrippsiella trochoidea* known as HABs causative species in Korea (Lee *et al.*, 2013). For this purpose, we generated a large dataset (N = 2,275) of remote sensing reflectance (R_{rs}) simulated under various bio-optical conditions using Hydrolight software with bio-optical data provided by the International Ocean-Color Coordinating Group (IOCCG). Using this dataset, we analyzed the characteristics of the R_{rs} spectra of blooms of *C. polykrikoides* and other species. Our results confirmed that the optical discrimination method based on two R_{rs} band ratios is compatible with current ocean color sensors and can be applied for detecting *C. polykrikoides* blooms in seawaters with various optical conditions.

Chapter 2 Data and Methods

2.1 Radiometric observations and discrete water samples

Hyperspectral radiometric measurements were conducted under non-bloom and *C. polykrikoides* bloom conditions between 25 and 31 August 2014 and between 31 August and 05 September 2015. These observations were performed in the southern coastal waters of Korea, where HABs have been frequented. The study area covered various optical conditions from Yeosu to Geoje, Korea (Fig. 4). A hyperspectral free-falling Profiler II (Satlantic LP, Canada) was used to measure the upwelling radiance ($L_u(\lambda)$) and downwelling irradiance ($E_d(\lambda)$) in the water column in the wavelength range 352-802 nm (Garaba & Zielinski, 2013). The remote sensing reflectance ($R_{rs}(\lambda)$) was then calculated from the method following the NASA protocols (Mueller, 2003). Additionally, surface water samples were collected for the determination of optical conditions in the bloom and non-bloom regions such as $a_{ph}(\lambda)$, Chl *a* concentration, CDOM absorption (a_g), and detritus/mineral absorption (a_{dm}). These *in situ* radiometric observations and bio-optical parameters were compared with $R_{rs}(\lambda)$ simulation data and $a_{ph}(\lambda)$ obtained from cultures.

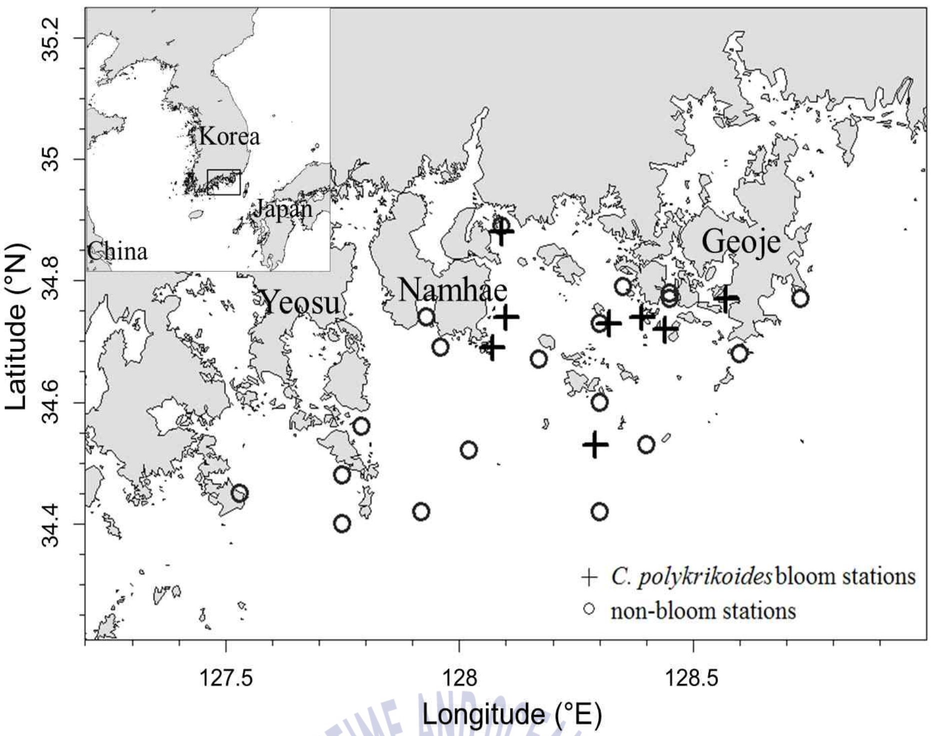

Fig. 4 Station map showing *C. polykrikoides* bloom stations (crosses) and non-bloom stations (circles) in the southern coastal waters of Korea.

2.2 Optical parameter measurements

2.2.1 Phytoplankton absorption and Chlorophyll *a*

Four dinoflagellate species (*C. polykrikoides, A. sanguinea, A. tamarense, and S. trochoidea*) have been known as the major causative species forming HABs in Korean coastal waters (Lee *et al.*, 2013). The four HABs species have morphologically different features (Fig. 5, Table 1). *A. sanguinea* was isolated from phytoplankton samples collected from waters of Yeosu, Korea, in August 2014; other species, including *C. polykrikoides*, were obtained from the Library of Marine Samples of the Korea Institute of Ocean Science and Technology (KIOST). The samples were cultured mono-specifically in enriched f/2 seawater medium (Guillard, 1975) at 18-22 °C and 32 PSU under constant light provided by a cool white fluorescent lamp with an irradiance of 250 $\mu E\ m^{-2}\ s^{-1}$ and 12:12 dark:light cycle. Culture samples were maintained in exponential growth and healthy states by transferring them with fresh media.

These culture samples were filtered to determine the spectral phytoplankton absorption coefficients, $a_{ph}(\lambda)$, of the four dinoflagellate species using a dual-beam spectrophotometer (Cary 300, Agilent) operating in the wavelength range 350-800 nm at 0.5 nm increments. Additionally, discrete water samples obtained during *C. polykrikoides* blooms and non-blooms (Fig. 4) were used to determine the $a_{ph}(\lambda)$ of natural phytoplankton assemblages. We employed the wet filter technique and calculated the final values of $a_{ph}(\lambda)$ following the ocean optics protocols of NASA (Mitchell *et al.*, 2003). Firstly, the optical density (O.D) of suspension samples were collected onto 25 mm Whatman GF/F paper under low vacuum to measure the total particulate absorption (a_p), and the two blanks were also collected from filtered seawater. Filter volumes of samples varied from 45 to 200 ml aliquots depending on the abundance of cells in the sample. The O.D of total particles on the filter was measured immediately after filtration. In the process of measurements, we made filter position as close as possible to the detector to prevent the loss of scattered light. The final values of O.D for sample filter were corrected for baseline and adjusted to zero in the near-infrared spectral region for null-points correction. We applied the method described in Roesler (1998) to correct the data for the path-length amplification effect (β factor). The a_p in $m^{-1}$is computed as

$$a_p(\lambda) = \frac{2.303A_f}{\beta V_f}[[O.D_{fp}(\lambda) - O.D_{bf}(\lambda)] - O.D_{null}] \tag{1}$$

Where A_f is the filter area on filter paper, V_f is the filter volume. $O.D_{fp}$ is the measured optical density of sample filter, $O.D_{bf}$ is the optical density of blank filter, and $O.D_{null}$ is a null wavelength residual correction from the infrared where particle absorption is minimal.

We also calculated the detritus absorption, $a_{dm}(\lambda)$, using Equation (1) by substituting $O.D_{fd}$ for $O.D_{fp}$. The $O.D_{fd}$ is the optical density of de-pigmented particle on filter paper that pigment were extracted in 100% methanol. Lastly, the $a_{ph}(\lambda)$ can be compute as the difference between $a_p(\lambda)$ and $a_{dm}(\lambda)$.

To calculate the phytoplankton absorption coefficient normalized to the Chl *a* concentration (a^*_{ph}), the Chl *a* concentration of each culture sample was measured from 90% acetone extracts using a fluorometer (Tuner Designs, 10-AU) according to Jeffrey and Humphrey (1975).

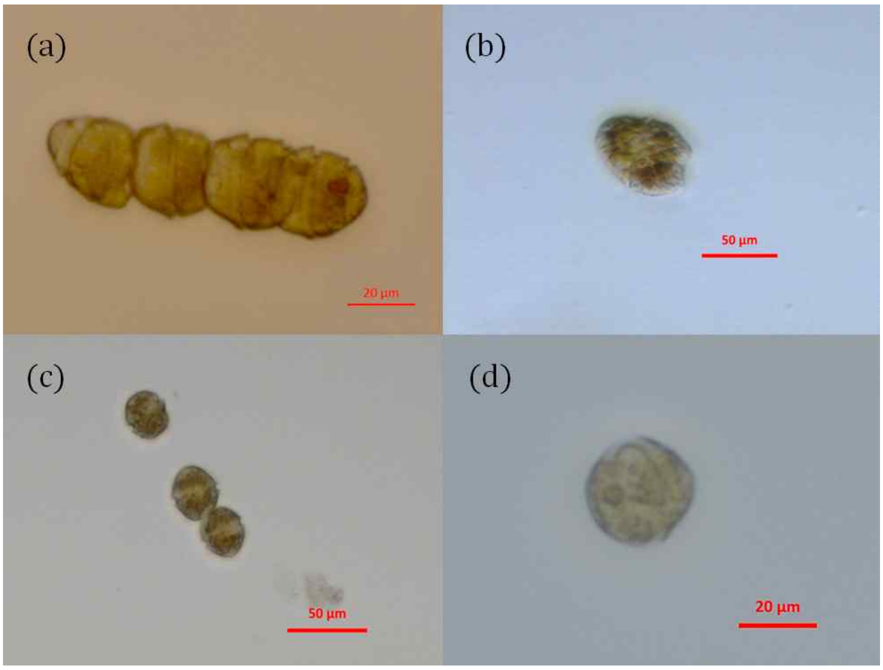

Fig. 5 Four dinoflagellate species isolated from the southern coastal waters of Korea. (a) *C. polykrikoides*, (b) *A. sanguinea*, (c) *A. tamarense*, and (d) *S. trochoidea*.

Table 1 Morphological features of the four dinoflagellate species causing HABs.

	C. polykrikoides	*A. sanguinea*	*A. tamarense*	*S. trochoidea*
Length	30 ~ 40 μm	40 ~ 80 μm	22 ~ 51 μm	16 ~ 36 μm
Width	22 ~ 30 μm	30 ~ 50 μm	17 ~ 44 μm	20 ~ 23 μm
Chain formation	> 4 cells	non-forming	solitary	non-forming
Type	naked (un-armored)	naked (un-armored)	armored	armored

2.2.2 Absorption of colored dissolved organic matter (CDOM)

To determine $a_g(\lambda)$ of discrete water samples obtained from field observations, seawater samples were filtered on 0.2 μm Whatman polycarbonate membrane. Absorbance of the filtered seawater was then measured in a 10 cm quartz cuvette at 0.5 resolution between 350 and 800 nm using a dual-beam spectrophotometer (Cary 300, Agilent). The mean value of the interval 590-600 nm was subtracted from the spectrum (baseline correction, Babin *et al.*, 2003) and the absorbance was then converted into an $a_g(\lambda)$. The spectral slope of a_g (S_g) was calculated using a nonlinear exponential fit function.

$$a_g(\lambda) = a_g(443)e^{-S_g(\lambda - 443)} \quad (2)$$

2.3 Hyperspectral R_{rs} simulation using Hydrolight

We performed numerical simulations using the radiative transfer model to simulate the subsurface light fields in a wide range of optical water conditions (Hydrolight version 5.1) (Mobley & Sundman, 2012). Specifically, $R_{rs}(\lambda)$ (in sr^{-1}) is defined as the ratio of the water-leaving radiance, $L_w(\lambda)$, to the downwelling irradiance, $E_d(\lambda)$ (see Eq. (3)). Because $R_{rs}(\lambda)$ can be expressed as a function of the total absorption and backscattering coefficients ($a(\lambda)$ and $b_b(\lambda)$, respectively) of the optical constituents, it can be written as Gordon *et al.* (1988):

$$R_{rs} = \frac{L_w(\lambda)}{E_d(\lambda)} \approx \frac{b_b(\lambda)}{a(\lambda)+b_b(\lambda)} \tag{3}$$

where $a(\lambda)$ and $b_b(\lambda)$ can be expressed as:

$$a(\lambda) = a_w(\lambda) + a_{ph}(\lambda) + a_g(\lambda) + a_{dm}(\lambda) \tag{4}$$

$$b_b(\lambda) = b_{bw}(\lambda) + b_{bph}(\lambda) + b_{bdm}(\lambda) \tag{5}$$

Here, the subscripts represent optically active constituents in seawater: pure water (w), phytoplankton (ph), CDOM (g), and detritus/mineral (dm). When performing Hydrolight simulations, the IOPs of optically active seawater constituents are required as inputs. The input data sources for the R_{rs} simulation were as follows: (1) the data derived from Pope and Fry, (1997) and Smith and Baker, (1981) were employed as the absorption (a_w) and backscattering (b_{bw}) coefficients for pure seawater, respectively. (2) The IOP data set, which has 500 different absorption and backscattering spectra (400–800 nm) of seawater constituents, such as phytoplankton, CDOM, and detritus/mineral, was obtained from the synthetic data assembled by the IOCCG (IOCCG, 2006; http://www.ioccg.org/groups/OCAG_data.html). These data were generated using bio-optical models based on extensive field measurements for algorithm test and/or comparison. Therefore, they can cover a wide range of variations in natural seawaters. (3) We used the a_{ph} spectra of the four HAB species, including *C. polykrikoides*, that were measured from the culture samples. In our simulations, we considered two types of a_{ph}: the measured a_{ph} spectra of the four HAB species and the a_{ph} spectra acquired from an IOCCG data set were used as representative of the HAB species and unspecified phytoplankton assemblages (UPA) in natural waters (Fig. 6), respectively. The simulations were conducted for five different Chl *a* concentrations, 5, 10, 15, 20, and 30 $\mu g\ l^{-1}$, to represent the initiation and the growth of the phytoplankton bloom.

To generate a large data set of $R_{rs}(\lambda)$ in various optical water conditions, the above inputs were combined. We chose the spectral slopes of $a_g(\lambda)$ and $a_{dm}(\lambda)$ (S_g and S_{dm}, respectively) to further simplify the simulations within a realistic range assuming that these slope were not correlated to the Chl *a* concentration (Kirk, 1994; Babin *et al.*, 2003). The 91 combinations were generated by $a_g(\lambda)$ and $a_{dm}(\lambda)$ (13 levels of $S_g \times 7$ levels of S_{dm} = 91 combinations) (Fig. 7). For each Chl *a* concentration, 91 a_{ph} spectra were selected randomly from the IOCCG database to create diverse absorption values associated with UPA. In total, 455 combinations of IOPs (five Chl *a* concentrations × 91 combinations) were used to simulate R_{rs}. These calculations were performed for the four HAB species and UPA.

The Hydrolight simulations were performed in the wavelength range 400–800 nm with a high spectral resolution and the input IOPs were maintained vertically constant. The sea surface boundary conditions were assigned with a wind speed of 5 m s^{-1} and the sky was assumed to be cloudless with a solar zenith angle of 30° (Wei *et al.*, 2016). Additionally, our simulations were set to run with inelastic scattering (Gokul & Shanmugam, 2016). Hydrolight provides two options that are commonly used for the phase function of particulate scattering. We used the more flexible Fournier-Forand phase function with b_{bph}/b_{ph} = 0.01 and b_{bdm}/b_{dm} = 0.018 (Mobley & Sundman, 2012; Tzorziou *et al.*, 2006). To consider uncertainties related to the backscattering of phytoplankton, we performed a sensitivity analysis using the backscattering ratios of phytoplankton 0.001, 0.005, 0.014, 0.02 and 0.05.

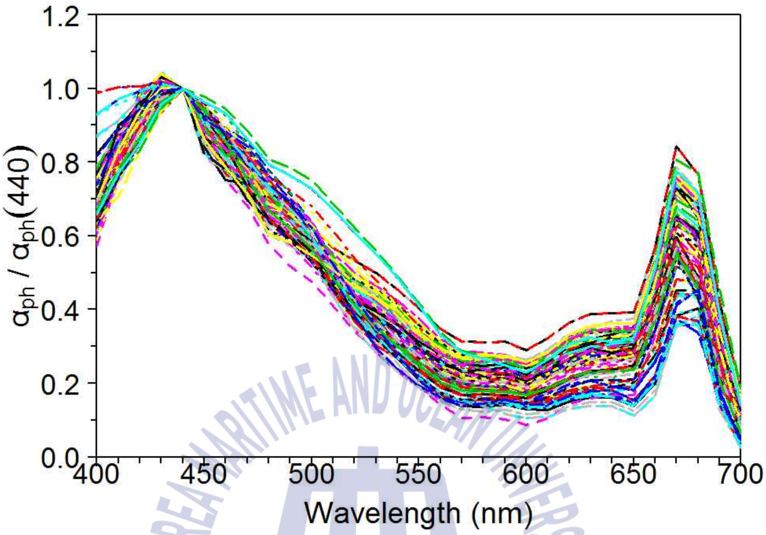

Fig. 6 The $a_{ph}(\lambda)$ normalized at 440 nm is taken from the IOCCG database. This graph indicates 125 spectra for five different Chl *a* concentrations (5, 10, 15, 20, and 30 $\mu g\ l^{-1}$).

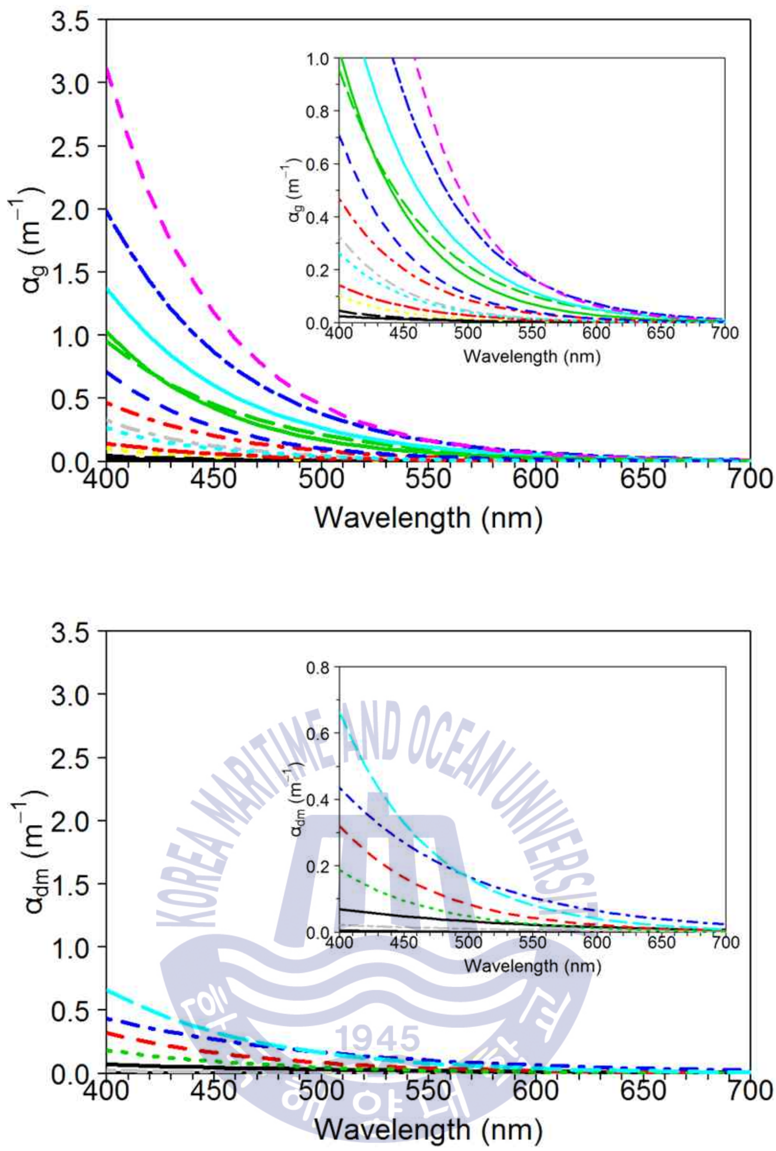

Fig. 7 The $a_g(\lambda)$ (n = 13) and $a_{dm}(\lambda)$ (n = 7) which were selected from the IOCCG database. Their combinations were used to create various optical conditions in the seawater.

2.4 Derivative analysis and similarity index

Derivative spectroscopy has been commonly used to analyze the similarities and differences in hyperspectral data (Xi et al., 2015; Tsai & Philpot, 1998) because it provides more detail information on the spectral shape corresponding to the spectral inflections. Derivative analysis enables spectra to be enhanced spectral inflections and small spectral features. In our study, second-derivative analysis was applied to the hyperspectral $a_{ph}(\lambda)$ and $R_{rs}(\lambda)$. Prior to derivative analysis, the measured $a_{ph}(\lambda)$ and simulated $R_{rs}(\lambda)$ were smoothed by cubic smoothing spline function in R program. Briefly, the second-derivatives were computed using spectra normalized to the respective spectral mean values. Bandwidth $(\triangle\lambda = \lambda_k - \lambda_j = \lambda_j - \lambda_i,\ \ \lambda_k > \lambda_j > \lambda_i)$ was selected for each data type to maximize the spectral signal to noise amplification.

$$\frac{d^2 s}{d\lambda^2} = \frac{d}{d\lambda}\left(\frac{ds}{d\lambda}\right) \approx \frac{s(\lambda_i) - 2s(\lambda_j) - s(\lambda_k)}{(\triangle\lambda)^2} \qquad (6)$$

The second-derivatives of $a_{ph}(\lambda)$ were used in a qualitative analysis to determine the wavelength positions of the absorption features of phytoplankton pigments. Additionally, we used the second-derivatives of $R_{rs}(\lambda)$ to quantify the spectral similarities in the R_{rs} spectra by adopting the spectral similarity index (SI) converted by arc-cosine transformation and division by $\pi/2$ (Kirkpatrick *et al.*, 2000; Millie *et al.*, 1997). We calculated the angle between two vectors comprising the second-derivative spectra of a standard *C. polykrikoides* and three dinoflagellates or UPA. The SI between two second-derivatives (e.g., *C. polykrikoides* and UPA) yielded a number between zero and one, where zero indicated no similarity and one denoted perfect similarity. This analysis was employed to determine useful information for discriminating R_{rs} between *C. polykrikoides* and other HAB species or UPA.

Chapter 3 Results

3.1 Light absorption of HAB species

Figure 8 shows the mean spectra of the Chl *a* specific absorption, $a^*_{ph}(\lambda)$, of the four cultured HAB species. The a^*_{ph} spectra exhibit some variability in magnitudes and spectral shapes from 400 to 700 nm. (1) The values of a^*_{ph} at 440 nm vary between 0.0192 (±0.0021) and 0.0328 (±0.0028) m^2 mg^{-1} and are within the range estimated in Prieur and Sathyendranath (1981) for *in situ* conditions. (2) Among the four species, *C. polykrikoides* absorbs relatively more light than the other species in the short wavelengths. (3) *S. trochoidea* shows a slightly larger peak at 465 nm than that at 440 nm, while for the other species the larger peak is at 440 nm. (4) The $a^*_{ph}(\lambda)$ of *C. polykrikoides* and *S. trochoidea* shows discernible slopes between 400 and 440 nm. In this wavelength range, *C. polykrikoides* and *S. trochoidea* have the steepest and the flattest slopes, respectively, among the four species.

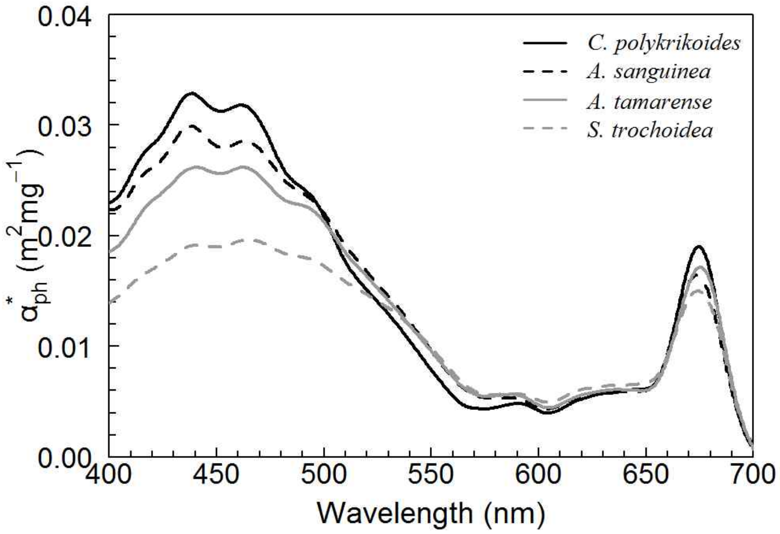

Fig. 8 Mean spectra of *in vivo* Chl *a* specific absorption of *C. polykrikoides* (n = 9), *A. sanguinea* (n = 10), *A. tamarense* (n = 10), and *S. trochoidea* (n = 11).

To determine the detailed differences and/or similarities between these spectra (Fig. 8), we calculated the second-derivative spectra from the mean normalized absorption of the four species (Fig. 9). These provided more detailed information on the spectral shape that corresponded to the spectral inflections of $a^*_{ph}(\lambda)$. Although differences are observed in magnitudes and spectral shapes among the cultured species (Fig. 8), the results of the second-derivative spectra analysis show that the inflexion positions do not differ significantly for the four cultured HAB species (Fig. 9(b)). The maxima and minima of the second-derivative spectra are located at similar wavelengths that correspond to the major pigments of the dinoflagellate species (Smith & Alberte, 1994; Bidigare *et al.*, 1989). In Fig. 9(a), four spectra exhibit major common absorption peaks at blue and red wavelengths owing to chlorophyll pigment absorption (Bricaud *et al.*, 1995) and low absorption at green wavelengths (approximately 600 nm). Furthermore, the absorption peaks and shoulders observed for the four species commonly occur at 440, 465, 495, and 675 nm. Especially, *C. polykrikoides* and *A. sanguinea* have very similar spectral patterns: these two are unarmored (athecate) species and both have similar cell size when *C. polykrikoides* makes the chains of multiple cells (Maldonado, 2008) (Table 1).

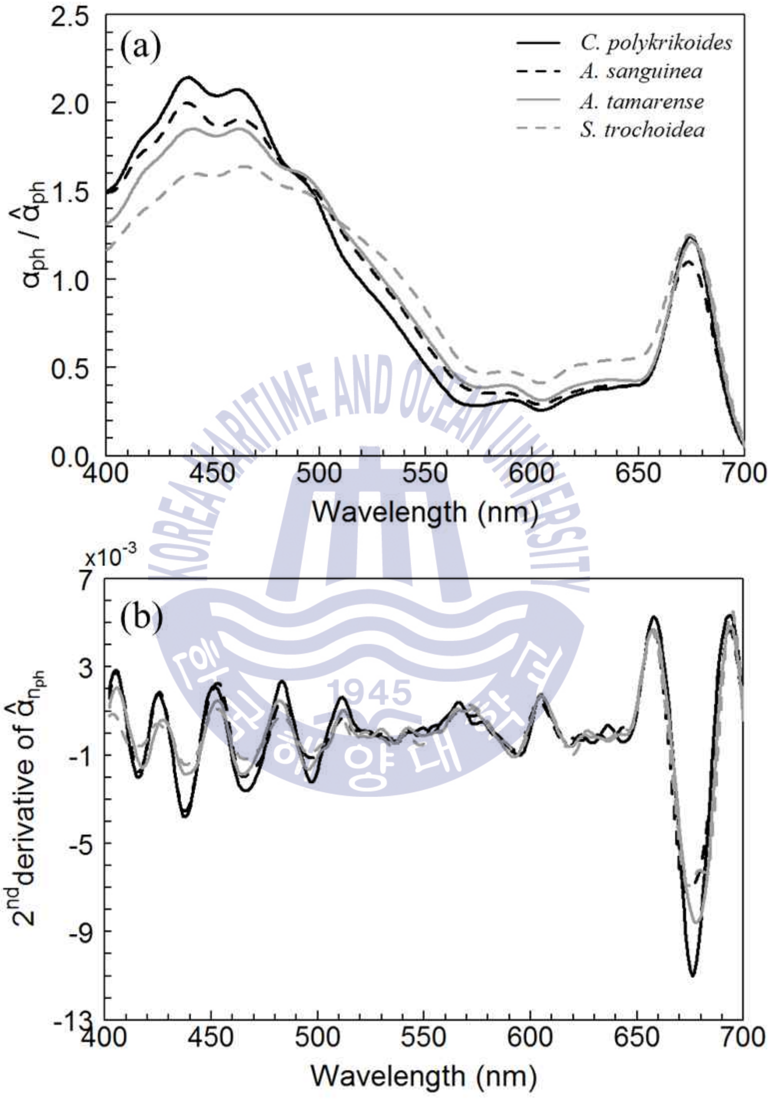

Fig. 9 (a) Representative mean normalized spectra, ($\hat{a}_{nph}(\lambda)$), (b) 2nd derivative spectra of the four dinoflagellate species.

As mentioned earlier, among the four species, *C. polykrikoides* has a high absorption value in the blue wavelength. This characteristic in the variation of a_{ph} seems consistent with increasing Chl *a* concentration. Figure 10 shows $a_{ph}(440)$ for the four cultured species as a function of Chl *a* concentration. The scattered points denote measurements of the same culture on different days and different dilutions. The a^*_{ph} spectra obtained on different days for each species are very similar (data not shown) and the relationship between $a_{ph}(440)$ and Chl *a* concentration remains mostly linear for all species under examined the experimental conditions (Sathyendranath *et al.*, 1987). The slope was estimated to be 0.0347 for *C. polykrikoides*, 0.0291 for *A. sanguinea*, 0.0255 for *A. tamarense*, and 0.0189 for *S. trochoidea*. The slope of *C. polykrikoides* was the largest among the four species.

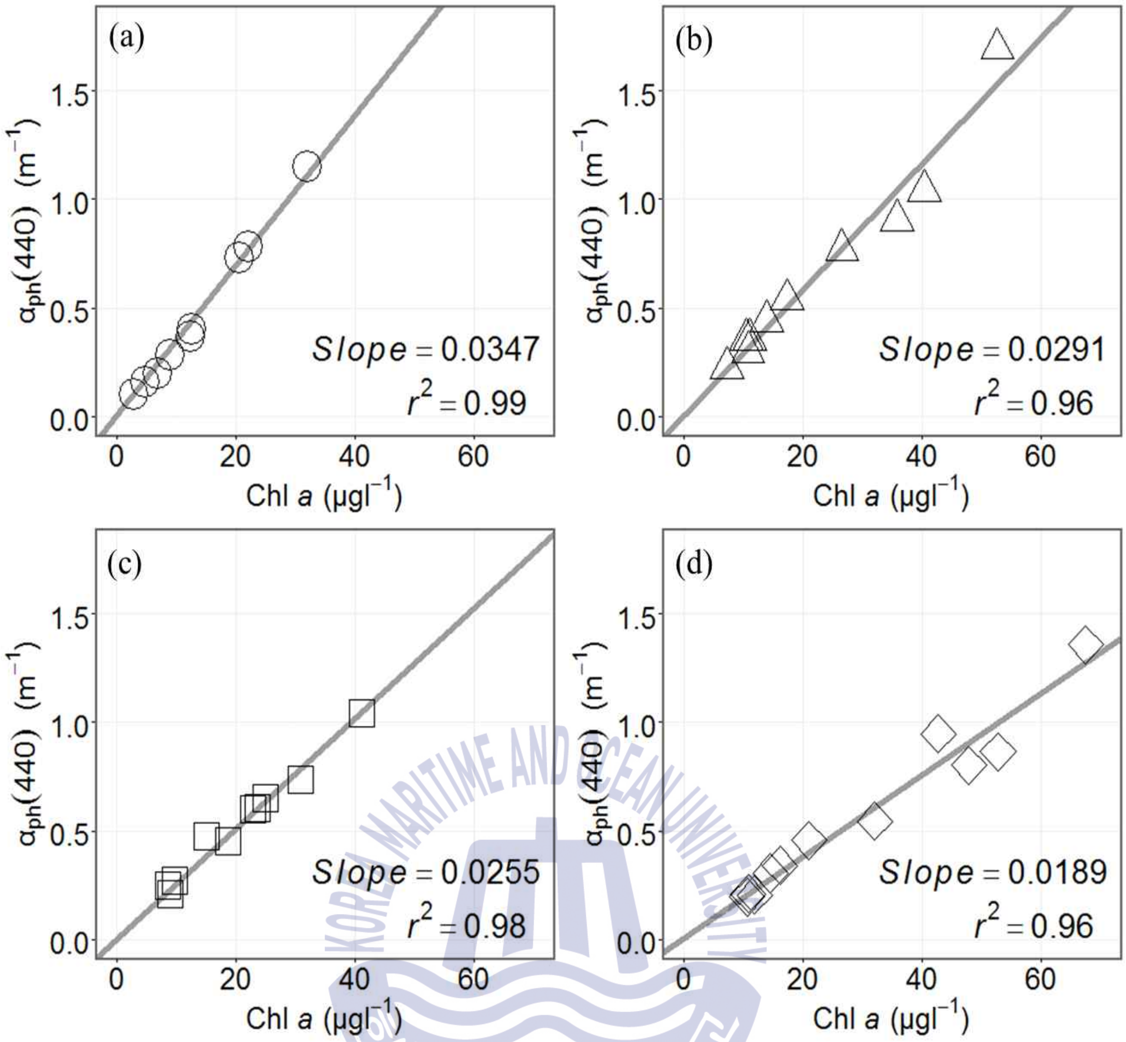

Fig. 10 Linear regression (without intercept) between the absorption coefficients of phytoplankton at 440 nm, $a_{ph}(440)$, and Chl *a* concentration for (a) *C. polykrikoides* (circles, n = 9), (b) *A. sanguinea* (triangles, n = 10), (c) *A. tamarense* (squares, n = 10) and (d) *S. trochoidea* (diamonds, n = 11). The slope and determination coefficient are shown in the lower right.

3.2 Comparison of a_{ph} in *in situ* and culture samples

We compared the $a_{ph}(\lambda)$ of the culture samples with that of *in situ* samples. Figure 11(a) shows the $a^*_{ph}(\lambda)$ normalized to 440 nm (hereafter referred to as "$a^*_{ph}(\lambda)/a^*_{ph}(440)$"), which were obtained during *C. polykrikoides* blooms and non-blooms in the southern coastal waters of Korea. Significant variations are observed in the magnitudes and spectral shapes of the calculated $a^*_{ph}(\lambda)/a^*_{ph}(440)$ that clearly indicate different types of a_{ph} between the *C. polykrikoides* bloom and non-bloom regions at approximately 465 nm. These differences were attributed to the bio-optical properties of phytoplankton assemblages and the dominant phytoplankton species [i.e., *C. polykrikoides* (>75%)] in the regions. The $a^*_{ph}(\lambda)/a^*_{ph}(440)$ of *C. polykrikoides* bloom regions was compared with that of *C. polykrikoides* cultured mono-specifically to examine their differences in the wavelength range 400-700 nm (Fig. 11(b)). To quantify this dissimilarity, we calculated the percentage difference (Craig *et al.*, 2006) between the spectral structures observed in the spectra of the *C. polykrikoides* bloom regions and the culture samples to be 2.3-6.4% with an average of 4.4%. In contrast, the spectral structures of the non-bloom regions and the cultured *C. polykrikoides* were clearly distinguishable with a mean difference of 16.0% (data not shown). We obtained the representative $a_{ph}(\lambda)$ of *C. polykrikoides* by combining the $a_{ph}(\lambda)$ acquired from the cultures with those from the bloom patches (Fig. 11 (b)).

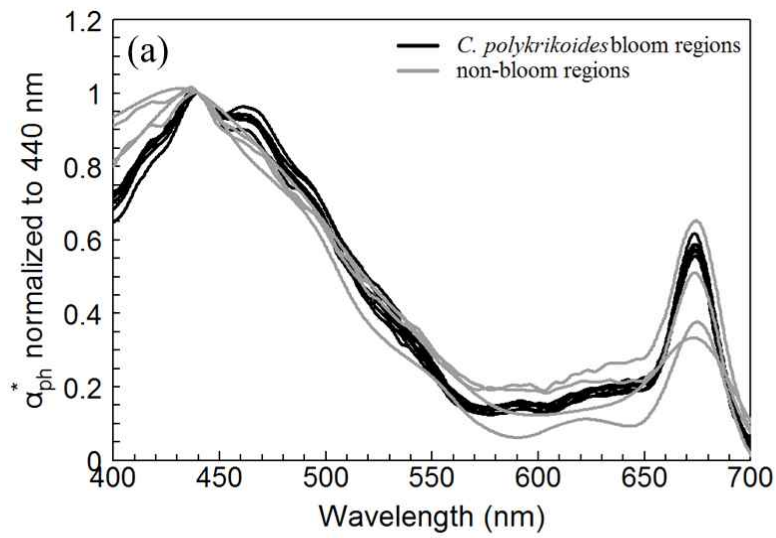

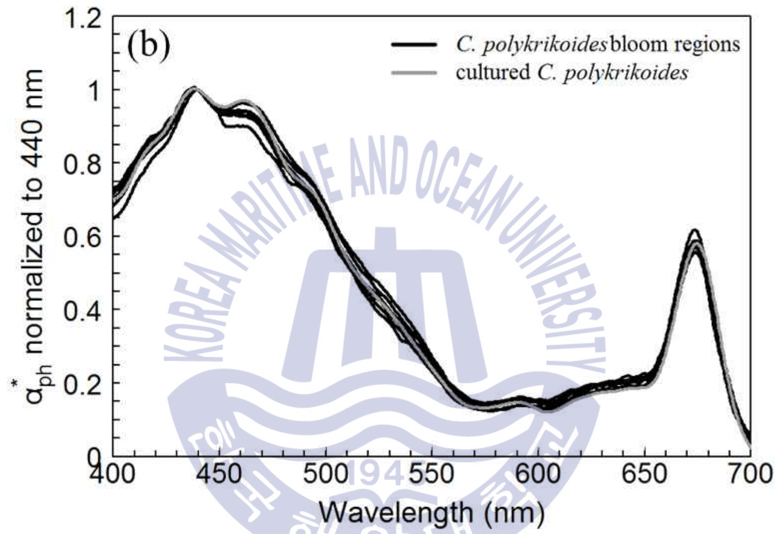

Fig. 11 Comparison of the $a^*_{ph}(\lambda)$ normalized to 440 nm ($a^*_{ph}(\lambda)/a^*_{ph}(440)$). (a) *C. polykrikoides* bloom (black) and non-bloom (grey) regions, and (b) *C. polykrikoides* cultured (grey) and *C. polykrikoides* obtained from bloom (black) regions.

3.3 Comparison of hyperspectral remote sensing reflectance (R_{rs})

3.3.1 *in situ* R_{rs} spectra

We compared the spectral characteristics of $R_{rs}(\lambda)$, which were obtained *in situ* measurements. Figure 12(a) and (b) show the R_{rs} spectra measured at *C. polykrikoides* bloom and non-bloom regions, respectively. Commonly, $R_{rs}(\lambda)$ increased from 400 to 570 nm, and then it started decreasing to 800 nm, except for a shoulder around 650 nm, and a peak (or shoulder) at 695 nm. This spectral pattern is indicative of typical coastal waters with phytoplankton, CDOM, and detritus/mineral (Maldonado, 2008). The $R_{rs}(\lambda)$ of two different regions are distinguished from each other in 400-800 nm, by the magnitude and spectral shapes.

Firstly, the bloom regions have lower reflectance than non-bloom regions because of the intensity of absorption for *C. polykrikoides* (Fig. 12). Actually, Chl *a* at non-bloom regions were estimated to be 0.459-11 $\mu g l^{-1}$, while Chl *a* at bloom regions were high values of 18-53 $\mu g l^{-1}$. Specifically, the magnitude of reflectance in the blue-green wavelengths shows very low value (Fig. 12 (a)). Secondly, $R_{rs}(\lambda)$ measured at bloom regions exhibit conspicuous two peaks around 570 and 695 nm and a distinct depression in the wavelength range of 400-590 nm. In contrast, $R_{rs}(\lambda)$ at non-bloom regions show one peak around 570 nm (i.e., with higher R_{rs} values along the short wavelengths and comparatively lower R_{rs} values at red wavelengths).

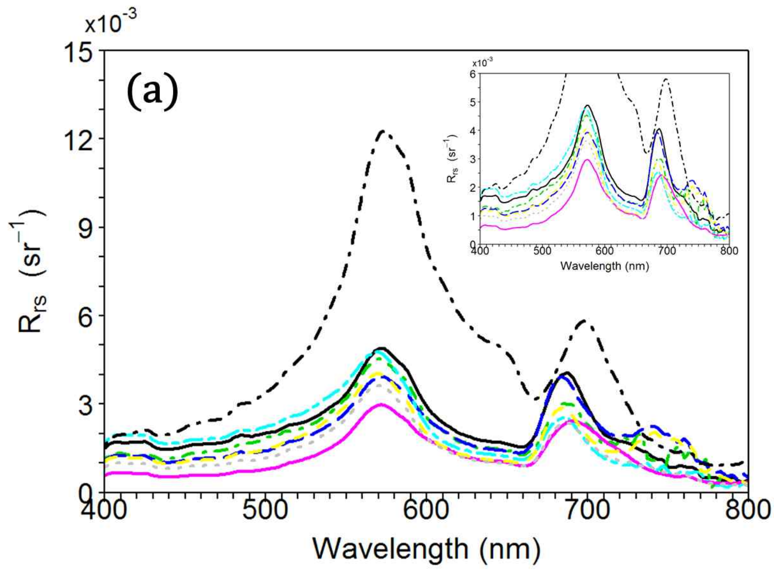

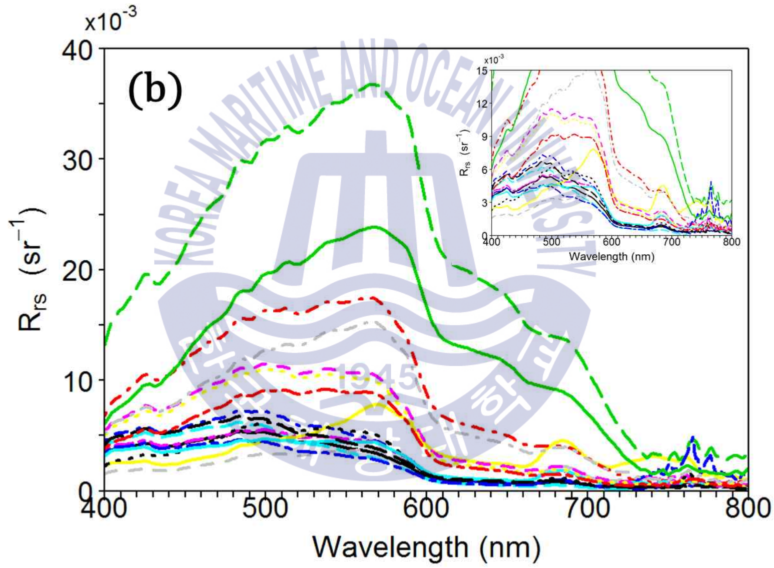

Fig. 12 The *in situ* R_{rs} spectra obtained from in-water radiometric measurements in (a) *C. polykrikoides* bloom and (b) non-bloom regions.

3.3.2 R_{rs} of HAB species and Unspecified Phytoplankton Assemblages

Figure 13(a) shows the R_{rs} spectra simulated using Hydrolight. The common features of the $R_{rs}(\lambda)$ of the four HAB species and UPA are: (1) a prominent peak near 570 nm (green peak), where backscattering processes prevail because of the weak phytoplankton absorption; (2) a distinct trough around 670 nm, and (3) a peak in the red/near-infrared (NIR) region at ~695 nm (the so-called red edge). These are nearly the same for the five groups and the second and third features are largely the outcome of the interaction between pure water and phytoplankton absorption (Gitelson *et al.*, 1999), (4) Small differences are observed in the red/NIR region, where pure water absorption is dominant.

The R_{rs} spectra that are based on the individual absorption spectra of the four dinoflagellate HAB species display very similar spectral inflexions (Fig. 13 (a)). The R_{rs} of the four HAB species at 30 $\mu g l^{-1}$ commonly exhibits stronger depression than that of UPA in the short wavelength region. The depression of the reflectance due to flat slope observed in 440-490 nm is, in turn, an outcome of the characteristics of $a_{ph}(\lambda)$ which are attributed to photosynthetic pigments of dinoflagellates (specifically, chlorophylls and carotenoids). This distinct feature of $R_{rs}(\lambda)$ becomes more pronounced with increasing Chl *a* concentration (Fig. 13(b)). The significant differences in the magnitudes and shapes of the R_{rs} spectra of the HAB species are not discernible for a similar concentration of Chl *a* (see details in Section 4.1). In contrast, the magnitudes and the shapes of the $R_{rs}(\lambda)$ of the HAB species show significant differences in comparison with those of UPA. The $R_{rs}(\lambda)$ of UPA is higher than that of the HAB species at a Chl *a* concentration of 30 $\mu g l^{-1}$ (Fig. 13(a)). This spectrum has steeper slopes in the wavelength range 440-490 nm in contrast with the R_{rs} spectra of the four HAB species.

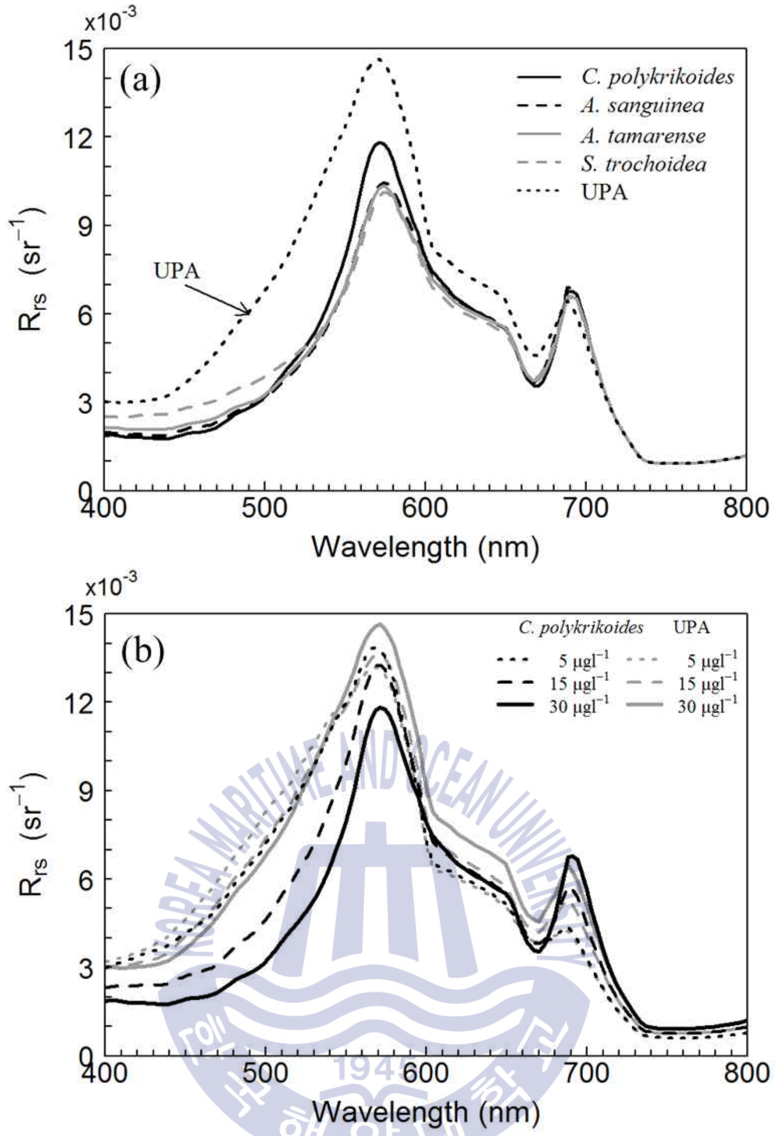

Fig. 13 Average of 91 R_{rs} spectra for (a) the four HAB species and UPA at a Chl *a* concentration of 30 $\mu g\ l^{-1}$, and (b) *C. polykrikoides* and UPA at 5, 15, and 30 $\mu g\ l^{-1}$.

3.3.3 Similarity index between *C. polykrikoides* and other species

To quantify the differences between the $R_{rs}(\lambda)$ spectra in the wavelength range 400-690 nm, the SI was calculated using the second-derivatives of R_{rs}. Derivative analysis and the SI approach to $R_{rs}(\lambda)$ were employed to provide useful information for the discrimination between the R_{rs} of *C. polykrikoides* and the three dinoflagellates or UPA. Figure 14(a) shows SIs calculated based on the second-derivatives at five Chl *a* concentrations from 5 to 30 $\mu g l^{-1}$. The SI between *C. polykrikoides* and the other HAB species indicated high similarity, as *C. polykrikoides* could not be distinguished from the other HAB species in the second-derivative spectra of R_{rs} (data not shown). At high Chl *a* concentration, they still yielded high similarity indices of approximately 0.90. However, with increasing Chl *a* concentration, the SI between *C. polykrikoides* and UPA decreased continuously and reached a minimum of 0.65 at a Chl *a* concentration of 30 $\mu g l^{-1}$. Therefore, the distinction of *C. polykrikoides* blooms from UPA using hyperspectral R_{rs} is possible at high level of Chl *a* owing to the low similarity in their second-derivative spectra. To determine the distinct differences [i.e., the depression shown in Fig. 13(a)] in the R_{rs} of the HABs and UPA, we calculated the SI in several wavelength bands based on MODIS wavebands (Fig. 14(b)), which were adopted to examine the applicability of satellite remote sensing data. The SI between *C. polykrikoides* and the other HAB species exhibits high a value of 0.83-0.97 near the 443, 488, 531, and 555 nm wavebands and is higher than the SI of *C. polykrikoides* versus UPA in all wavebands. In the 443 and 488 nm wavebands, the SI of UPA has a particularly low value of 0.70 and 0.62, respectively.

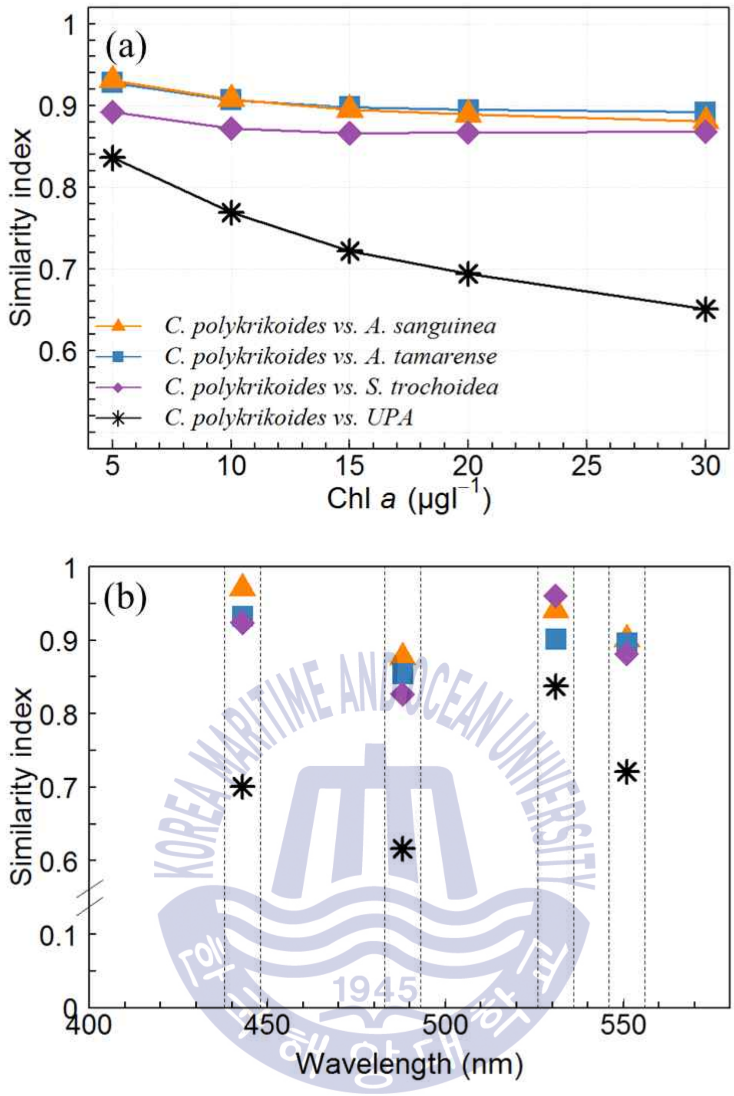

Fig. 14 SIs of the second-derivatives of $R_{rs}(\lambda)$ between *C. polykrikoides* and other species (a) with varying Chl *a* concentrations in the wavelength range 400-690 nm and (b) at several MODIS wavebands (443, 488, 531, and 555 nm) with a Chl *a* concentration of 30 $\mu g\ l^{-1}$.

3.4 Optical discrimination of *C. polykrikoides* from other species

The differences in the spectral shape of R_{rs} for *C. polykrikoides* and UPA strongly suggest that it can be used to differentiate the two groups (Fig. 13). The most conspicuous differences can be observed in the slope of the blue-green range (440-600 nm): the R_{rs} curve of *C. polykrikoides* is flatter in the blue range but steeper than that of UPA in the green region. This spectral difference can be summarized by comparing the slope in the two parts of the R_{rs} curves. To achieve this, we tested different R_{rs} ratios [$R_{rs}(\lambda_2)/R_{rs}(\lambda_1)$] of bands centered at λ_2 and λ_1 ($\lambda_1 < \lambda_2$). Considering the potential applications of satellite remote sensing, we used MODIS wavelengths. We constructed the $R_{rs}(\lambda)$ of two hypothetically mixed assemblages, namely, *C. polykrikoides*-dominated blooms (80% of *C. polykrikoides* and 20% UPA) and 100% UPA, which represent typical phytoplankton assemblages under natural conditions (Millie *et al.*, 1997). Simulations of $R_{rs}(\lambda)$ were performed for two phytoplankton groups at the various concentrations of Chl *a* (5-30 $\mu g l^{-1}$) under optically complex conditions with varying CDOM and detritus/mineral concentrations. To select the optimal bands that effectively depict the changes in the slope, we calculated the latter against increasing Chl *a* for all band combinations. The best combinations were determined to be R_1: $R_{rs}(555)/R_{rs}(531)$ and R_2: $R_{rs}(488)/R_{rs}(443)$; R_1 showed the most rapid increase and R_2 the fastest decrease with increasing Chl *a* in case of *C. polykrikoides*-dominated blooms. From the simulated $R_{rs}(\lambda)$, we calculated the R_{rs} ratios, $R_{rs}(\lambda_2)/R_{rs}(\lambda_1)$, and used them to plot the data points (Fig. 15). In the R_1-R_2 space R_1 increases with Chl *a* because the slope of R_{rs} in the green band increases; however, R_2 shows no sensitivity to Chl *a* (the color shading in Figure 15 denotes Chl *a* concentrations). At a low Chl *a* concentration of 5 $\mu g l^{-1}$, the *C. polykrikoides* data points are separated from those of UPA. As Chl *a* increases, both groups exhibit higher R_1. As a result, UPA points at higher Chl *a* concentrations occupy the same space as the *C. polykrikoides* points at lower Chl *a* concentrations. However, the observed increases in the R_1 of both groups with increasing Chl *a* are disproportionate and for a the Chl *a* concentration above 15 $\mu g l^{-1}$, the data points of the *C. polykrikoides* blooms completely separate from those of UPA despite the variability of the optical water types with various combinations of CDOM and detritus/mineral.

The ideal approach to validating the model is the comparison between the *in situ* and simulated reflectance values at each station. However, this was not practically possible because the water samples were not obtained synchronously with the optical measurements. During the *in situ* optical measurements, the density of *C. polykrikoides* was continuously changing owing to the small-scale patch structure and the movement of currents. Therefore, a substantial mismatch occurred between the optical profiling and the water sampling, which hindered a precise comparison at each station. Instead, we made a bulk comparison of *in situ* reflectance and simulated reflectance in Figure 15, which shows that the *in situ* band ratios are consistent with simulated ones: (1) Both the *in situ* *C. polykrikoides* blooms and non-bloom regions fall within the range of simulated band ratios. (2) *C. polykrikoides* blooms were clearly separated from non-blooms similarly in simulations and the *in situ* measurements. (3) The *in situ* band ratios, in both non-bloom and bloom stations, occupy lower R_2 regions, which is consistent with our interpretation that R_2 variability is determined by CDOM absorption (see Section 4.2 for further discussion). Our *in situ* conditions were characterized by relatively lower CDOM absorption. The ranges of the important bio-optical parameters measured *in situ* mostly fell within those used in the simulations (Table 2). The range of $a_g(443)$ used in the simulations was much wider than that of the *in situ* values. Taken together, the model seems to simulate the *in situ* reflectance reasonably well.

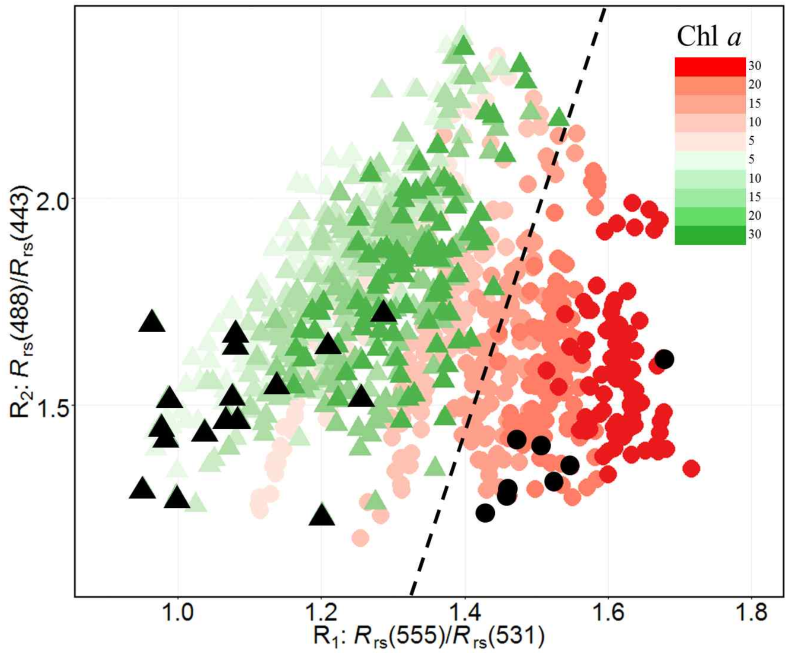

Fig. 15 Relationship between simulated R_1 and R_2 of *C. polykrikoides* (red circles) and UPA (green triangles) with varying Chl *a* concentrations from 5 to 30 μg l^{-1}. The black symbols indicate the *in situ* observations of *C. polykrikoides* blooms (circles) and non-bloom areas (triangles) areas.

Table 2 Ranges of parameters of the model and field data.

Parameters	Model inputs	Field data	
	IOCCG synthetic data	Non-bloom regions	*C. polykrikoides* bloom regions
Chl *a*	5 ~ 30 $\mu g l^{-1}$	0.459 ~ 11 $\mu g l^{-1}$	18 ~ 53 $\mu g l^{-1}$
$a_g(443)$	0.015 ~ 1.430 m^{-1}	0.027 ~ 0.148 m^{-1}	0.027 ~ 0.228 m^{-1}
$a_{dm}(443)$	0.003 ~ 0.378 m^{-1}	0.003 ~ 0.261 m^{-1}	0.035 ~ 0.171 m^{-1}

Chapter 4 Discussion

We simulated the R_{rs} spectra of the four dinoflagellates and UPA under various optical conditions. The $R_{rs}(\lambda)$ of *C. polykrikoides* and the three dinoflagellates species show similar spectral shapes and, consequently cannot be easily distinguished (Fig. 13(a)). However, the R_{rs} spectra of the *C. polykrikoides* and UPA were discriminated from each other because of spectral differences in the short wavelengths (Fig. 14(b)). These differences can be effectively summarized by using the two band ratios of R_{rs}. The waters dominated by *C. polykrikoides* (80%) and UPA (100%) clearly occupy separate subspaces in the two-dimensional space of R_1 and R_2 (Fig. 15). While the greatest separation was observed between *C. polykrikoides* and UPA, the other dinoflagellates occupied different spaces between those of *C. polykrikoides* and UPA (data not shown). This suggests that the two R_{rs} ratios R_1 and R_2 are the most efficient ratios to separate optical signatures between *C. polykrikoides* and UPA. These simulations were conducted within realistic range of CDOM and detritus/mineral (Babin *et al.*, 2003). The results suggest that the discrimination of *C. polykrikoides* blooms using R_{rs} is plausible under natural conditions.

4.1 Similarity of $R_{rs}(\lambda)$ characteristics among dinoflagellate HAB species

The optical discrimination approach using the R_{rs} band ratio is similar to the findings of Shang *et al.* (2014), which proposed the optical discrimination between dinoflagellates from diatoms based on R_{rs}. The optical differences were attributed to the phytoplankton absorption properties. Consequently, the contribution of the phytoplankton absorption properties by the major accessory pigments to the differences in $R_{rs}(\lambda)$ is crucial in understanding the optical discrimination of *C. polykrikoides*.

The measured $a_{ph}(\lambda)$ of *C. polykrikoides* reveals several absorption peaks and shoulders in the short wavelengths (Fig. 8). The peak observed near 440 nm corresponds to an absorption maximum of predominantly Chl *a* (Jeffrey & Vesk, 1997). The peak at 465 nm is the combined absorption maximum of chlorophyll c_2 and peridinin, which are synchronously detected as typical pigments of dinoflagellates (Bidigare et al., 1989; Maldonado, 2008). The R_{rs} spectra that were simulated using the measured $a_{ph}(\lambda)$ of *C. polykrikoides* show a strong depression in the wavelength range 440-490 nm due to the influence of the high pigment absorption at 465 nm [described in Section 3.3.2, Fig. 13(a)]. This depression gets stronger (flattened slope between 440 and 490 nm) with increasing pigment absorption (Fig. 13(b)) and could be an important factor in the discrimination of *C. polykrikoides* from UPA.

Unfortunately, other dinoflagellate species (*A. sanguinea, A. tamarense and S. trochoidea*) exhibit similar spectral absorption properties to *C. polykrikoides* (Fig. 9(b)). They have similar pigment composition containing chlorophyll c_2 and carotenoids (i.e., peridinin, diadinoxanthin, dinoxanthin, diatoxanthin, and β-carotene), which appear to be unique to dinoflagellates (Maldonado, 2008; Liu *et al.*, 2014; Bustillos-Guzmán *et al.*, 2004). From the results of this study, the high SI (of the order of 0.90) between *C. polykrikoides* and the other three HAB species indicates that the four HABs have similar spectral characteristics in a wide range of Chl *a* concentration (Fig. 14(a)). This caused the difficulty in differentiating individual phytoplankton species blooms among the four dinoflagellate species that form HABs.

4.2 Distribution of *C. polykrikoides* blooms and UPA in R_{rs} ratio space

We analyzed a large simulated $R_{rs}(\lambda)$ data set (n = 2,275) using the derivative analysis/SI approach. As a result, the HAB species were easily distinguished from UPA with increasing Chl *a* concentration. Especially, *C. polykrikoides* were clearly discriminated by the magnitude of a_{ph} at 465 nm in Figure 8. The R_{rs} at specific wavebands also exhibited clear differences between *C. polykrikoides* and UPA. As shown in Figure 15, the simulation results indicate that *C. polykrikoides* is well separated from UPA in the R_{rs} ratio space. In general, the R_{rs} ratios associated with *C. polykrikoides* show larger R_1 than UPA. This distribution pattern covers a wide range of optical conditions (Table 2). In contrast, the scattering of the points along R_2 direction represent variations due to CDOM (see below).

As the Chl *a* concentration increases from 5 to 30 $\mu g l^{-1}$, all the scattered points of the two phytoplankton groups in the R_{rs} ratios space move toward larger R_1. Especially, the R_1 of *C. polykrikoides* covers a wider range than that of UPA (Fig. 16). This is because the absorption properties influenced by the pigment composition affect the reflectance (Mao *et al.*, 2010). The R_{rs} ratios of *C. polykrikoides* reflect the influence of typical pigments in the wavelength range 440-490 nm, as described in Section 3.3.1. In this range, as R_{rs} is reduced by enhanced absorption, the slopes of $R_{rs}(\lambda)$ are flattened in response to the increasing pigment concentrations. Therefore, the high R_1 (i.e., steep variation) of *C. polykrikoides* is accompanied by low R_2 (i.e., flattened slope) that is attributed to the influence of high a_{ph} in the wavelength range 440-490 nm.

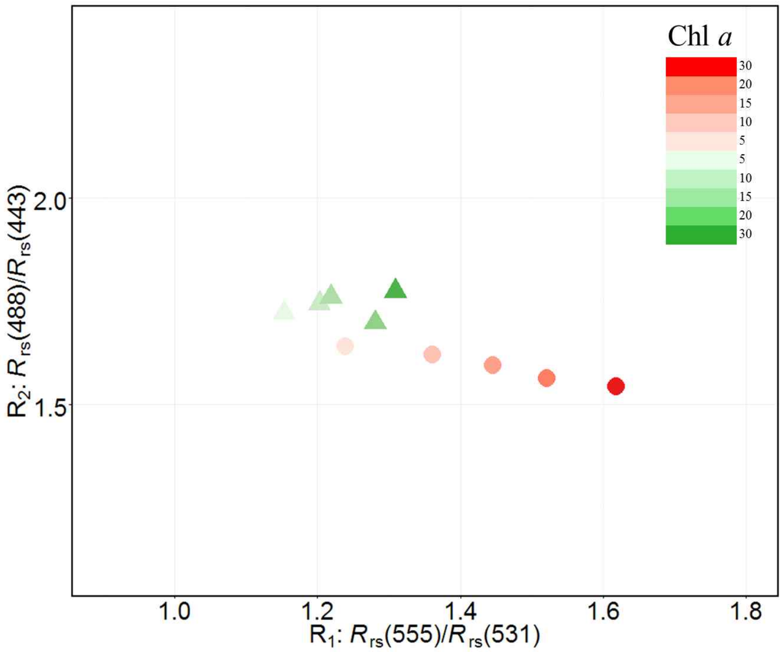

Fig. 16 Average of 91 R_{rs} ratios of the data points in Figure 14 at different Chl *a* concentrations (5, 10, 15, 20, and 30 $\mu g\ l^{-1}$). The red circles and green triangles denote *C. polykrikoides* and UPA, respectively.

At the same Chl *a* concentration, the R_{rs} ratios are distributed along the R_2 axis (Fig. 17). This result is attributed to the variation of CDOM absorption (a_g). As $a_g(443)$ increases, the R_{rs} ratios move towards higher R_2. While the strong influence of a_g causes further reduction in the R_{rs} spectra, the slope in the blue region could increase. As an optically active constituent of seawater, CDOM absorbs light predominantly in the blue end of this wavelength range and its spectrum declines exponentially with wavelength (Kirk, 1994; Babin *et al.*, 2003). This absorption characteristic of CDOM influences the R_{rs} spectra. Since $a_g(443)$ is always higher than $a_g(488)$, $R_{rs}(443)$ becomes disproportionately lower than $R_{rs}(488)$ and hence R_2 becomes larger as CDOM increases. This distribution pattern was also observed in the space of the *in situ* R_{rs} ratios (Fig. 15). Son *et al.* (2011) suggested that *C. polykrikoides* bloom waters in the southern coast of Korea are relatively less influenced by CDOM and detritus.

Although our simulations were performed using a wide range of $a_g(443)$, our *in situ* observations were conducted in waters with low $a_g(443)$ below 0.228 m^{-1} (Table 2).

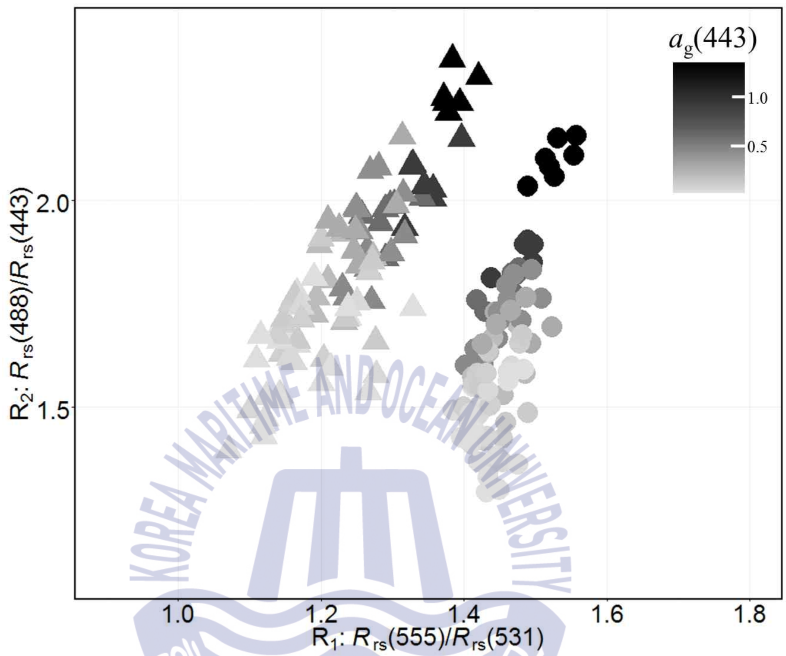

Fig. 17 Distribution of R_{rs} ratios with increasing $a_g(443)$ for a constant concentration of Chl *a* (15 $\mu g\ l^{-1}$)

4.3 Uncertainties in the simulation

We used the simulated R_{rs} to cover a wide range of bio-optical conditions. The simulations required various parameters as described in Section 2.3. Therefore, uncertainties in the parameters could be a critical issue in the interpretation of the simulation results. The measured $a_{ph}(\lambda)$ of *C. polykrikoides* under different culture conditions were consistent with those of the *in situ* water samples from *C. polykrikoides* bloom regions. The $a_{ph}(\lambda)$ of UPA were obtained from the IOCCG synthetic data (500 spectra) (Fig. 6), which are obtained from an absorption spectra data bank composed of the extensive measurements representing oligotrophic to eutrophic natural environments (Lee, 2003). $a_g(\lambda)$, $a_{dm}(\lambda)$, and $b_{bdm}(\lambda)$ were modeled to cover a wide range of values reported for various environments. Therefore, these parameters seem to be suitable for performing simulations. However, the backscattering coefficient of phytoplankton was the most uncertain parameter in our simulations because few such measurements have been performed and reported. To our knowledge, the only study that has measured the backscattering coefficient of *C. polykrikoides* reported that the backscattering ratio was in the range 0.01-0.022 (digitized from their Fig. 23 and 25) for cultures with Chl *a* concentration ranging from 1.96 to 17.62 $\mu g l^{-1}$ (n = 10) (Maldonado, 2008). The ratio of backscattering to the total scattering for phytoplankton was selected as 0.01 which is the most commonly used in previous studies. Throughout the entire wavelength range, a constant value of b_{bph}/b_{ph} was applied to total scattering to obtain the backscattering coefficients (Lee, 2003). To examine how the uncertainty in b_{bph}/b_{ph} could affect our results, we conducted a sensitivity analysis (Table 3). We compared the band ratios of R_{rs} from runs using the standard backscattering ratio and from runs using altered values. The mean absolute percentage difference (APD) was used to evaluate the sensitivity performance of the backscattering ratio. The sensitivity analysis indicated that the backscattering ratio had no effect on the R_{rs} band ratios and thus no effect on the discrimination of *C. polykrikoides* blooms from UPA. With respect to the original R_{rs} ratios of both *C. polykrikoides* and UPA, the APD obtained from the sensitivity analysis was below 5.95%. We conclude that the uncertainties in the model parameters in particular, the backscattering ratio do not alter the model outputs and the discrimination of *C. polykrikoides* blooms from UPA blooms.

Table 3 Mean APD, used for evaluating the sensitivity of R_1 and R_2 to the variation of the backscattering ratio of phytoplankton.

b_{bph}/b_{ph}	*C. polykrikoides*		UPA	
	R_1	R_2	R_1	R_2
0.001	4.12%	5.34%	3.03%	5.95%
0.005	1.27%	2.04%	1.06%	2.03%
*0.01				
0.014	0.79%	0.94%	0.62%	0.91%
0.02	1.79%	1.80%	1.35%	1.91%
0.05	5.21%	3.53%	3.67%	5.17%

*Standard value used in the simulation.

Chapter 5 Conclusion

We investigated the possibility of optically discriminating *C. polykrikoides* blooms from non-dinoflagellate blooms or non-bloom conditions based on simulated R_{rs} spectra covering a wide range of optical conditions. The $a_{ph}(\lambda)$ of dinoflagellate *C. polykrikoides* in the wavelength range 400–500 nm showed discernible absorption features, which resulted from the combined absorption maxima of chlorophyll c_2 and peridinin. These distinct characteristics of a_{ph} are translated into a depressed R_{rs} in the blue-green region for *C. polykrikoides*, while no similar depression was observed for UPA. The two R_{rs} band ratios, R_1 and R_2 were determined to be most effective for capturing these characteristics. In the space of the two ratios, *C. polykrikoides* was separated from UPA for various optical conditions. Among the four dinoflagellates, *C. polykrikoides* was best discriminated from UPA because it exhibited the highest a^*_{ph} (Fig. 8). Because the four dinoflagellate species have a similar set of photosynthetic pigments, they showed similar spectral shapes and consequently were not clearly separated in the R_1–R_2 space except in high Chl *a* concentrations. Additionally, the distinction between *C. polykrikoides* and UPA was difficult at low Chl *a* concentrations because of the reduced effect of a_{ph} under the influence of other optically active constituents. However, the discrimination of *C. polykrikoides* blooms from those of UPA seems possible when the concentration of Chl *a* is sufficiently high (conservatively, greater than 15 $\mu g l^{-1}$). The simulation results were consistent with *in situ* observations; this suggests that our results are sufficiently robust despite the uncertainties in the backscattering ratio. The sensitivity analysis on this parameter also supports our argument.

This approach can be extended to other dinoflagellate species; however the sensitivity of detection range would be different from that of *C. polykrikoides*. Although our study primarily targeted Korean coastal waters, the results can be applied to other geographical regions, as our approach is not based on empirical relationships and our simulation covers a much wider range of bio-optical conditions. To apply this approach to *C. polykrikoides* bloom detection, further work is required in the future. Specifically, the development of algorithms based on the two ratios is necessary to discriminate *C. polykrikoides* in natural conditions. As Figure 15 shows, many combinations of varying densities of UPA and *C. polykrikoides* can exist, which would result in overlapping R_{rs} ranges for actual blooms. Simple techniques such as discriminant functions or clustering are not effective in this situation. Artificial intelligence techniques, such as artificial neural network, could be more effectively implemented in such cases. Such algorithms can be used for in-water optical measurements for the automatic detection of dinoflagellate blooms and can be extended for application in satellite ocean color sensors. However, in coastal waters, where HABs are truly problematic, the atmospheric correction of satellite ocean color data remains still a standing issue, particularly in the blue bands (Mouw *et al.*, 2015). If the errors in retrieving R_{rs} are significant, an algorithm based on our results will not function as efficiently. Therefore, the issues in the atmospheric correction must be resolved for the application of this method to the satellite detection of HABs in coastal waters.

Acknowledgements

At the end of my thesis I would like to thank all those people who made this thesis possible and an unforgettable experience for me.

First of all, I would like to express my sincere gratitude to my professor, Dr. Sinjae Yoo at the KIOST, who offered continuous advice and encouragement throughout the course of this thesis. He put into training me in the scientific field and encouraged me to grow as an independent thinker. So, I got the opportunity to develop my own individuality and self-sufficiency by being allowed to work with such independence. I have learned many things since I became Dr. Yoo's student.

I would also like to express my deep grateful to Dr. Young Baek Son for his assistance and guidance whenever I was in need.

In addition Dr. Dongseon Kim deserve special thanks, as my thesis committee member and advisor.

I am thankful to Dr. Taehee Lee and members of Marine Ecosystem Dynamics Laboratory with whom I had the opportunity to work. A special thanks goes to Su-In Kim, Soonmi Lee, and Soeon Ahn. They have encouraged me to endure this course to the end and have been supportive in the research.

Life at graduate insititute is not always wonderful. Nevertheless, it is lucky for me to meet some congenial friends who inspirit my effort to overcome these difficulties. These friends are Boeun Cho, Joo Young Jeon.

Finally, and most importantly, I would like to express the deepest gratitude to my family which includes my parents, two sisters, and a brother-in-law for their unflagging support and unconditional love throughout my life and my studies. Without their encouragement and support, it is impossible for me to finish the course of this thesis.

References

Ahnm Y.H. & Shanmugam, P., 2006. Detecting the red tide algal blooms from satellite ocean color observations in optically complex Northeast-Asia Coastal waters. Remote Sens. Environ. 103(4), 419-437.

Alvain, S., Moulin, C., Dandonneau Y. & Loisel, H., 2008. Seasonal distribution and succession of dominant phytoplankton groups in the global ocean: A satellite view. Global Biogeochem. Cy. 22(3).

Babin, M. et al., 2003. Variations in the light absorption coefficients of phytoplankton, nonalgal particles, and dissolved organic matter in coastal waters around Europe. J. Geophys. Res. 108(C7).

Bidigare, R.R., Morrow, J.H. & Kiefer, D.A., 1989. Derivative analysis of spectral absorption by photosynthetic pigments in the western Sargasso Sea. J. Mar. Res. 47(2), 323-341.

Bricaud, A., Babin, M., Morel, A. & Claustre, H., 1995. Variability in the chlorophyll-specific absorption coefficients of natural phytoplankton: Analysis and parameterization. J. Geophys. Res. 100(C7), 13321-13332.

Bustillos-Guzmán, J., Gárate-Lizárraga, I., López-Cortés, D. & Hernández-Sandoval, F., 2004. The use of pigment "fingerprints" in the study of harmful algal blooms. Rev. Biol. Trop. 52, 17-26.

Cannizzaro, J.P. et al., 2008. A novel technique for detection of the toxic dinoflagellate, *Karenia brevis*, in the Gulf of Mexico from remotely sensed ocean color data. Cont. Shelf Res. 28(1), 137-158.

Choi, J.K. et al., 2014. Harmful algal bloom (HAB) in the East Sea identified by the Geostationary Ocean Color Imager (GOCI). Harmful Algae 39, 295-302.

Craig, S.E. et al., 2006. Use of hyperspectral remote sensing reflectance for detection and assessment of the harmful alga, *Karenia brevis*. Appl. Opt. 45(21), 5414-5425.

Garaba, S.P. & Zielinski, O., 2013. Comparison of remote sensing reflectance from above-water and in-water measurements west of Greenland, Labrador Sea, Denmark Strait, and west of Iceland. Opt. Express. 21(13), 15938-15950.

Gitelson, A.A. et al., 1999. Comparative reflectance properties of algal cultures with manipulated densities. J. Appl. Phycol. 11(4), 345-354.

Gobler, C.J. et al., 2012. The role of nitrogenous nutrients in the occurrence of harmful algal blooms caused by *Cochlodinium polykrikoides* in New York estuaries (USA). Harmful Algae. 17, 64-74.

Gokul, E.A. & Shanmugam, P., 2016. An optical system for detecting and describing major algal blooms in coastal and oceanic waters around India. J. Geophys. Res. Oceans. 121, 1953-1969.

Gordon, H.R. et al., 1988. A semianalytic radiance model of ocean color. J. Geophys. Res. 93(D9), 10909.

Guillard,, R.R.L., 1975. Culture of phytoplankton for feeding marine invertebrates. in Culture of marine invertebrate animals, Smith, W.L. & Chanley, M.H., ed. (Springer US), pp. 29-60.

Guzmán, L., Varela, R., Muller-Karger, F. & Lorenzoni, L., 2016. Bio-optical characteristics of a red tide induced by *Mesodinium rubrum* in the Cariaco Basin, Venezuela. J. Mar. Syst. 160, 17-25.

Hu, C. et al., 2005. Red tide detection and tracing using MODIS fluorescence data: A regional example in SW Florida coastal waters. Remote Sens. Environ. 97(3), 311-321.

IOCCG, 2000. Remote sensing of Ocean Colour in Coastal, and Other Optically-Complex, waters. in Reports of the International Ocean-Colour Coordinating Group, No. 3, Sathyendranath, S. ed. (IOCCG Dartmouth, NS).

IOCCG, 2006. Remote sensing of Inherent Optical Properties: Fundamentals, Tests of Algorithms, and Applications. in Reports of the International Ocean-Colour Coordinating Group, No. 5, Lee, Z.P. ed. (IOCCG Dartmouth, NS).

Ishizaka, J. et al., 2006. Satellite detection of red tide in Ariake Sound, 1998–2001. J. Oceanogr. 62(1), 37-45.

Jeffrey, S.W. & Humphrey, G.F., 1975. New spectrophotometric equations for determining chlorophyll a, b, c_1 and c_2 in higher plants, algae and natural phytoplankton. Biochem. Physiol. Pflanz. 167, 191-194.

Jeffrey, S.W. & Vesk, M., 1997. Introduction to marine phytoplankton and their pigment signatures. in Phytoplankton Pigments in Oceanography, Jeffrey, S.W., Mantoura, R.F.C. & Wright, S.W., ed. (UNESCO), pp. 37-84.

Kirk, J.T.O., 1994. Light and photosynthesis in aquatic ecosystems. (Cambridge university press).

Kirkpatrick, G.J., Millie, D.F., Moline, M.A., & Schofield, O., 2000. Optical discrimination of a phytoplankton species in natural mixed populations. Limnol. Oceanogr. 45(2), 467-471.

Kurekin, A.A., Miller, P.I. & Van der Woerd, H.J., 2014. Satellite discrimination of *Karenia mikimotoi* and *Phaeocystis* harmful algal blooms in European coastal waters: Merged classification of ocean colour data. Harmful Algae. 31, 163-176.

Lee, C.K., Park, T.G., Park, Y.T. & Lim, W.A., 2013. Monitoring and trends in harmful algal blooms and red tides in Korean coastal waters, with emphasis on *Cochlodinium polykrikoides*. Harmful Algae. 30, S3-S14.

Lee, C.K., Park, Y.G., Park, T.G., & Suh, Y.S., 2014. Economic losses to the aquaculture industry by harmful algal blooms in Korea since 2001. PICES Scientific Report No. 47, 35-40.

Lee, Z.P., 2003. Models, parameters, and approaches that used to generate wide range of absorption and backscattering spectra. (IOCCG).

Liu, S. et al., 2014. HPLC pigment profiles of 31 harmful algal bloom species isolated from the coastal sea areas of China. J. Ocean U. China 13(6), 941-950.

Lubac, B. et al., 2008. Hyperspectral and multispectral ocean color inversions to detect *Phaeocystis globosa* blooms in coastal waters. J. Geophys. Res. 113(C6).

Maldonado, D.J.C., 2008. Spectral properties and population dynamics of the harmful dinoflagellate *Cochlodinium polykrikoides* (Margalef) in southwestern Puerto Rico. Ph. D. Thesis, University of Puerto Rico.

Mao, Z. et al., 2010. Effects of phytoplankton species composition on absorption spectra and modeled hyperspectral reflectance. Ecol. Inform. 5(5), 359-366.

Millie, D.F. et al., 1997. Detection of harmful algal blooms using photopigments and absorption signatures: A case study of the Florida red tide dinoflagellate, *Gymnodinium breve*," Limnol. Oceanogr. 42(5, part2), 1240-1251.

Mitchell, B.G., Kahru, M., Wieland, J., & Stramska, M., 2003. Determination of spectral absorption coefficients of particles, dissolved material and phytoplankton for discrete water samples. in Ocean optics protocols for satellite ocean color sensor validation, Rev. 4, Vol. IV, Mueller, J.L, Fargion, G.S. & McClain, C.R. ed. (NASA

Goddard Space Flight Center, Greenbelt, MD).

Mobley, C.D. & Sundman, L.K., 2012. HydroLight 5.1 EcoLight 5.1 Users' Guide. Sequoia Scientific, Inc.

Mouw, C.B. et al., 2015. Aquatic color radiometry remote sensing of coastal and inland waters: Challenges and recommendations for future satellite missions. Remote Sens. Environ. 160, 15-30.

Mueller, J.L., 2003. In-water radiometric profile measurements and data analysis protocols. in Ocean Optics Protocols for Satellite Ocean Color Sensor Validation, Rev. 4, Vol. III, J. L Mueller, G. S. Fargion & C. R. McClain ed. (NASA Goddard Space Flight Center, Greenbelt, MD).

O'Reilly, J.E. et al., 2000. Ocean color chlorophyll a algorithms for SeaWiFS, OC2, and OC4: Version 4. in SeaWiFS postlaunch calibration and validation analyses, Part 3, Hooker, S.B. & Firestone, E.R., ed. (NASA Goddard Space Flight Center, Greenbelt, MD), pp. 9-27.

Pope, R.M. & Fry, E.S., 1997. Absorption spectrum (380-700 nm) of pure water. II. Integrating cavity measurements. Appl. Opt. 36(33), 8710-8723.

Prieur, L. & Sathyendranath, S., 1981. An optical classification of coastal and oceanic waters based on the specific spectral absorption curves of phytoplankton pigments, dissolved organic matter, and other particulate materials. Limnol. Oceanogr. 26(4), 671-689.

Roelke, D.L., Kennedy, C.D. & Weidemann, A.D., 1999. Use of discriminant and fourth-derivative analyses with high-resolution absorption spectra for phytoplankton research: Limitations at varied signal-to-noise ratio and spectral resolution. Gulf Mex. Sci. 17(2), 75-86.

Roesler, C.S., 1998. Theoretical and experimental approaches to improve the accuracy of particulate absorption coefficients derived from the quantitative filter technique. Limnol. Oceanogr. 43(7), 1649-1660.

Sasaki, H. et al., 2008. Optical Properties of Red Tide in Isahaya Bay, Southwestern Japan: influence of chlorophyll a concentration. J. Oceanogr. 64, 511-523.

Shang, S. et al., 2014. A new approach to discriminate dinoflagellate from diatom blooms from space in the East China Sea. J. Geophys. Res. 119(7), 4653-4668.

Sathyendranath, S., Lazzara, L. & Prieur, L., 1987. Variations in the spectral values of specific absorption of phytoplankton. Limnol. Oceanogr. 32(2), 403-415.

Siswanto, E., Ishizaka, J., Tripathy, S.C. & Miyamura, K., 2013. Detection of harmful algal blooms of *Karenia mikimotoi* using MODIS measurements: A case study of Seto-Inland Sea, Japan. Remote Sens. Environ. 129, 185-196.

Smith, C.M. & Alberte, R.S., 1994. Characterization of in vivo absorption features of chlorophyte, phaeophyte and rhodophyte algal species. Mar. Biol. 118(3), 511-521.

Smith, R.C. & Baker, K S., 1981. Optical properties of the clearest natural waters (200 -800 nm). Appl.Opt. 20(2), 177-184.

Son, Y.B. et al., 2011. *Cochlodinium polykrikoides* red tide detection in the South Sea of Korea using spectral classification of MODIS data. Ocean Sci. J. 46(4), 239-263.

Stumpf, R.P. et al., 2003. Monitoring *Karenia brevis* blooms in the Gulf of Mexico using satellite ocean color imagery and other data. Harmful Algae. 2,:147-160.

Suh, Y.S., Jang, L.H., Lee, N.K. & Ishizaka, J., 2004. Feasibility of red tide detection around Korean waters using satellite remote sensing. J. Fish. Sci. Tech. 7(3), 148-162.

Tomlinson, M.C. et al., 2004. Evaluation of the use of SeaWiFS imagery for detecting *Karenia brevis* harmful algal blooms in the eastern Gulf of Mexico. Remote Sens. Environ. 91(3-4), 293-303.

Tsai, F. & Philpot. W., 1998. Derivative analysis of hyperspectral data. Remote Sens. Environ. 66(1), 41-51.

Tzortziou, M. et al., 2006. Bio-optics of the Chesapeake Bay from measurements and radiative transfer closure. Estuar. Coast. Shelf Sci. 68(1-2), 348-362.

Wei, J. et al., 2016. Spectral slopes of the absorption coefficient of colored dissolved and detrital material inverted from UV-visible remote sensing reflectance. J. Geophys. Res. Oceans 121(3), 1953-1969.

Wynne, T.T. et al., 2008. Relating spectral shape to cyanobacterial blooms in the Laurentian Great Lake. Int J Remote Sens. 29, 3665-3672.

Xi, H. et al., 2015. Hyperspectral Differentiation of Phytoplankton Taxonomic Groups: A Comparison between Using Remote Sensing Reflectance and Absorption Spectra. Remote Sens. 7(11), 14781-14805.

Appendix A Model input data

A.1 The a_w and b_{bw} used to simulation R_{rs} spectra

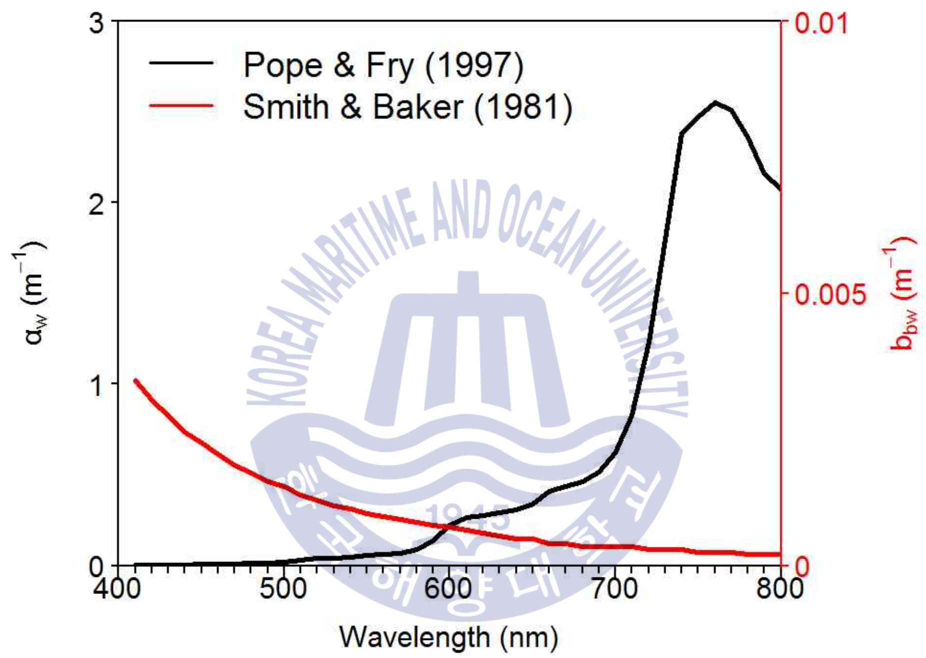

Fig. A1 The absorption and backscattering coefficients of pure water.

A.2 The absorption coefficient at 443 nm and slope of a_g and a_{dm}

Number	a_g		a_{dm}	
	$a_g(443)$ (m^{-1})	S_g (nm^{-1})	$a_{dm}(443)$ (m^{-1})	S_{dm} (nm^{-1})
1	0.015	0.0124	0.0032	0.0147
2	0.239	0.0168	0.0166	0.0071
3	0.526	0.0149	0.0520	0.0074
4	1.021	0.0166	0.1880	0.0133
5	0.711	0.0164	0.1095	0.0135
6	1.430	0.0194	0.2972	0.0096
7	0.046	0.0196	0.3783	0.0140
8	0.149	0.0195		
9	0.023	0.0170		
10	0.074	0.0163		
11	0.501	0.0179		
12	0.332	0.0189		
13	0.125	0.0186		